KERNFORSCHUNGSANLAGE JÜLICH GmbH

Institut für Nukleare Sicherheitsforschung

Modelling of Steam Condensation in the Primary Flow Channel of a Gas-Heated Steam Generator

by

H. Kawamura, G. Meister

Jül - Spez - 174
Oktober 1982
ISSN 0343-7639

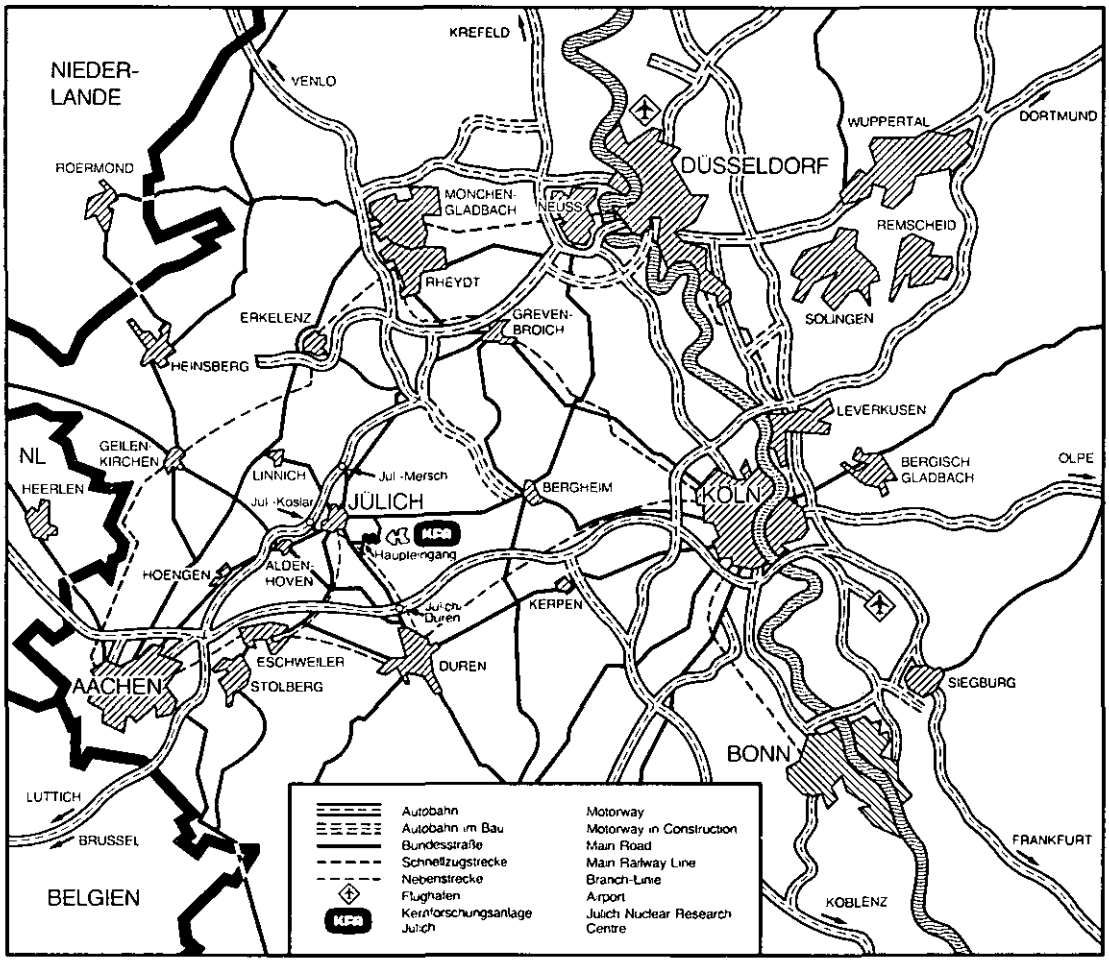

Als Manuskript gedruckt

Spezielle Berichte der Kernforschungsanlage Jülich — Nr. 174

Institut für Nukleare Sicherheitsforschung Jül - Spez - 174

Zu beziehen durch: ZENTRALBIBLIOTHEK der Kernforschungsanlage Jülich GmbH

Postfach 1913 · D-5170 Jülich (Bundesrepublik Deutschland)

Telefon: 02461/610 · Telex: 833556 kfa d

Modelling of Steam Condensation in the Primary Flow Channel of a Gas-Heated Steam Generator

by

H. Kawamura, G. Meister

Modelling of Steam Condensation in the Primary Flow Channel of a Gas-Heated Steam Generator

by

H. Kawamura, G. Meister

Abstract

A new simulation code has been developed for the analysis of steam ingress accidents in high temperature reactors which evaluates the heat transfer in a steam generator heated by a mixture of helium and water steam. Special emphasis is laid on the analysis of steam condensation in the primary circuit of the steam generator.

The code takes wall and bulk condensation into account. A new method is proposed to describe the entrainment of water droplets in the primary gas flow.

Some typical results are given. Steam condensation in the primary channel may have a significant effect on temperature distributions. The effect on the heat transferred by the steam generator, however, is found to be not so prominent as might be expected. The reason is discussed.

A simplified code will also be described, which gives results with reasonable accuracy within much shorter execution times. This code may be used as a program module in a program simulating the total primary circuit of a high temperature reactor.

MODELLIERUNG DER DAMPFKONDENSATION IM PRIMÄR-STRÖMUNGSKANAL EINES GASBEHEIZTEN DAMPFERZEUGERS

von

H. Kawamura, G. Meister

ZUSAMMENFASSUNG

Es wird ein neues Simulationsprogramm beschrieben, welches für die Analyse von Dampf-Einbruch-Störfällen in Hochtemperatur-Reaktoren entwickelt wurde. Es beschreibt den Wärmeübergang in einen Dampferzeuger, der durch eine Mischung aus Helium und Wasserdampf beheizt wird. Schwerpunkt der Entwicklung ist die Analyse möglicher Dmapfkondensation im Primärkanal des Dampferzeugers.

Das Programm berücksichtigt Wand- und Volumenkondensation. Es enthält ein neues Modell für den Transport von Wassertropfen im Primär-Gasstrom.

Einige typische Ergebnisse werden vorgestellt und diskutiert. Es zeigt sich, daß Dampfkondensation im Primärkanal die Temperaturverteilung erheblich verändern kann. Der Einfluß auf die vom Dampferzeuger übertragene Leistung ist jedoch geringer, als man erwarten würde. Der Grund hierfür wird diskutiert.

Es wird außerdem ein Programm, basierend auf einem vereinfachten Modell beschrieben, welches vergleichbare Ergebnisse bei wesentlich geringerem Rechenzeitbedarf liefert. Dieses Programm wurde als Programm-Baustein entwickelt, welcher in einem größeren Rechenprogramm, welches den gesamten Primärkreislauf eines Hochtemperaturreaktors simuliert, verwendet werden kann.

Contents

Acknowledgements

The authors would like to acknoledge the support and interest by Dr. J. Fassbender, invaluable discussion by Dr. W.Rehm, and great help by Miss R.Finken and by Mrs. N.Tietz.

This study was made during the first author's stay in KFA as a resident officier of KFA/JAERI collaboration in the field of the HTR development. He wish also to express his appreciation gratefully to Dr. P.Engelmann, a member of board, to Dr. N.Kirch and Dr. M.Helmbold of HTA, and to Dr. W. von Lensa and Mrs. M.L.Schüller of PTH for the good and unforgettable collaboration during his stay in Jülich.

1. Introduction

In case of a tube rupture in a steam generator of a high temperature reactor plant steam and/or water will ingress into the primary helium circuit. Since the pressure on the secondary side of the steam generator is much higher than the pressure of the primary circuit the ingress will cause a pressure build-up. Moreover chemical reactions beteewn the core graphite and the steam transported to the core are possible. This kind of accident, therefore, requires careful investigation with regard to its consequences.

The total amount of steam or water which may enter the primary system in case of a failure of one steam generator is limited in practice due to certain design provisions. Additionally several safety devices exist, which are designed to interrupt the ingress. In a hypothetical accident, however, where, for instance, the failure of the active safety devices has to be assumed, rather large amounts of steam may enter the primary system. In this case the primary pressure may increase to such an extent that the integrity of the pressure vessel will become endangered. If the removal of the heat generated in the core can be maintained anyway, a situation may arise after some time, where the steam partial pressure at some point in the primary circuit will exeed the local saturation pressure. Steam condensation then becomes possible and a decrease of the rate of pressure rise may be expected. Condensation in the primary system, therefore, is an important process to be considered if the consequences of this kind of accident are analysed.

The location in the primary circuit where condensation starts is the economizer part of a steam generator, because its heat exchanging surface forms the coldest surface in the system. Moreover, the total amount of the condensate depends on the cooling capability of the steam generator since the latent heat released by condensation must be removed form the system.

The modelling of steam condensation in the primary flow channel of a gas heated steam generator and the simulation program based on this model as described below is assumed to be applicable to various types of HTR steam generators. The layout of the steam generator underlying the present study refers to that of the THTR.

The design for the steam generator used in the THTR plant adopts an upward gas and downward steam/water flow. So the question arises whether the water condensed in the primary circuit flows upwards together with the gas or falls downwards opposite to the gas flow.

Another question is how the water film condensed on a cooled tube surface will behave. The cooled surface is not a smooth vertical tube as often assumed in classical analysis of the condensation. In the present case the surface is formed by a complicated bundle of tubes. So, some simplification is required. The cooled surface is replaced by a smooth surface with a proper assumption of liquid entrainment.

There is also a problem regarding the heat transfer coefficient of the condensate water film. A lot of studies have been made on this point, especially on the condensation of saturated vapor. In this case, the main heat resistance exists in the condensate film. So, the condensation rate is mainly controlled by this resistance. In the present case, however, a large amount of noncondensable gas exists. So, the controlling process is the mass transfer of steam in the non-condensable gas. This study has shown that the thermal resistance of the water film is of much less importance.

In the following part of this paper, the calculation model and the corresponding formule are described; then calculated results and the effect of some parameters are discussed. The model developed is based on physically proper assumptions but is fairly sophisticated.

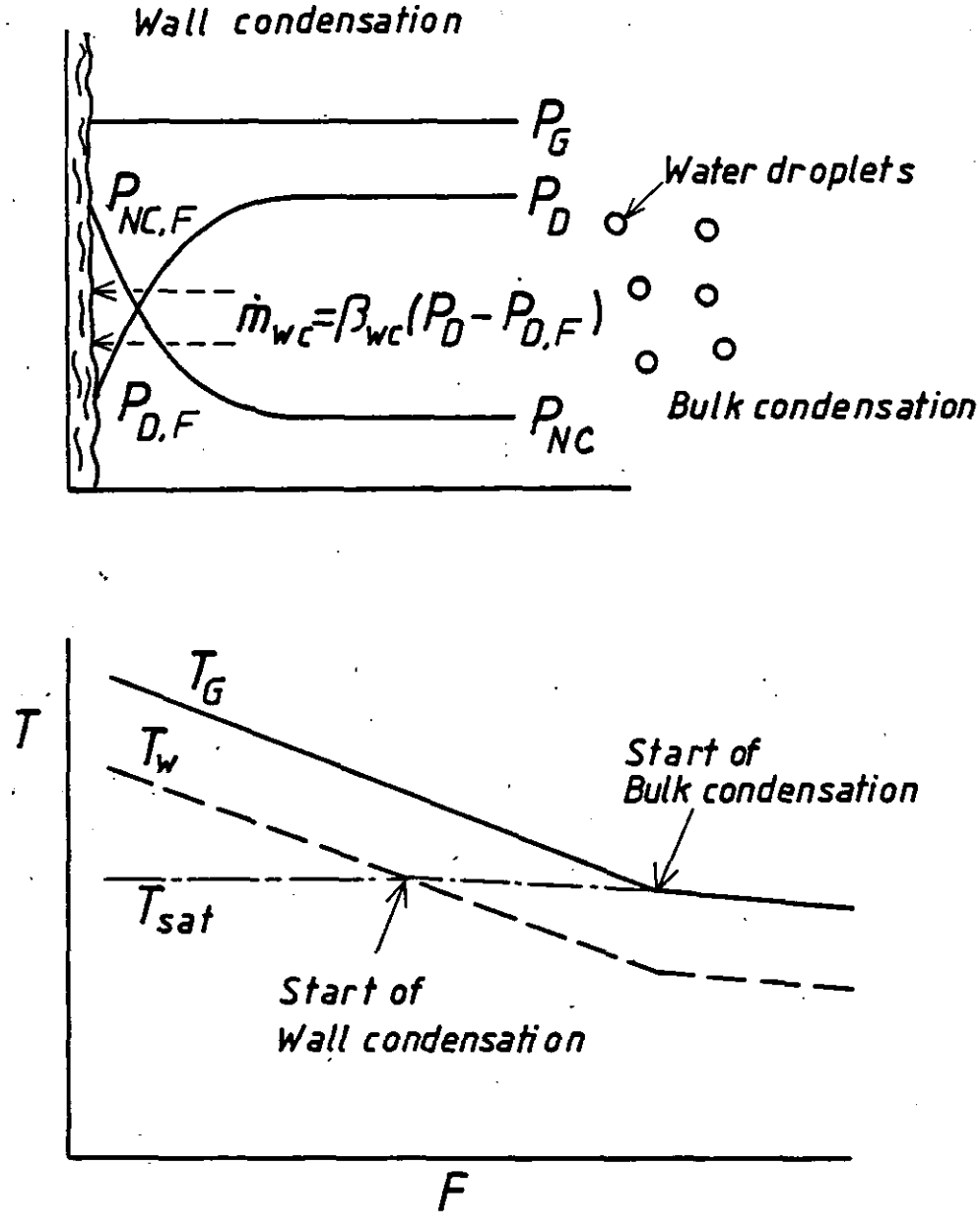

Fig. 1: Model of wall and bulk condensation

2. Modelling of Condensation Phenomena

2.1 Condensation

Two types of condensation are taken into account in the present analysis (see. Fig. 1 a).

(a) Wall condensation

This is the formation of a water film over a cooled tube wall. It occurs if the wall temperature T_W becomes lower than the saturation temperature T_{sat} corresponding to the partial pressure of the steam.

The wall-condensation rate is determined by the mass transfer of the steam through the non-condensable gas such as helium. The mass flow density of steam is given by

$$\dot{m}_{WC} = \beta_{WC} (P_D - P_{D,F}) \tag{2.1}$$

where β_{WC} is the mass transfer coefficient and $P_{D,F}$ the steam partial pressure at the film surface. The mass transfer coefficient can be obtained from the similarity of heat and mass transfer[1]. Details of the calculation is given in Appendix I.

(b) Bulk condensation

When the bulk gas temperature T_G becomes equal to or decreases below the saturation temperature, then the steam component starts to condense in the bulk gas. The condensed water formed here is assumed to be water fog floating in the gas. It is also assumed that the water droplets and the steam are always in thermal equilibrium, that is, no subcooling is required for the fog formation in the gas. The subcooling depends on the number of nuclei in the gas. In this case, however, many water droplets exist already before the start of the bulk condensation because of entrainment of the film as described later. These water droplets will act as nuclei for the fog formation, so the assumption of the equilibrium appears to be reasonable in this case. The process assumed is shown schematically in Fig. 1 b. The gas and wall temperatures T_g and T_W decrease in flow direction.

The wall condensation starts first, and then the bulk condensation. After the start of the bulk condensation, T_G and T_{sat} remain to be equal owing to the assumption of the equilibrium condition.

2.2 Direction of film flow

Two different forces act on the water film formed over the tube surface, that is, the gravity g and the shear stress due to the gas flow τ_F. Since the steam generator design often adopts an upward gas flow, these two forces act in the opposite direction (see Fig.2). Thus, if τ_F is large enough, the film will flow upwards; while if τ_F is small, the film will flow downwards following the gravity.

The momentum equation for the film is

$$\mu \frac{d^2u}{dy^2} = \rho g \sin\phi \qquad (2.2)$$

The boundary conditions are

$$u = 0; \quad y = 0$$

$$\mu \frac{du}{dy} = \tau_F; \quad y = \delta$$

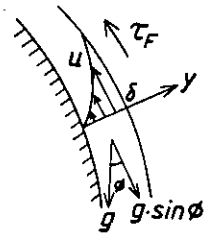

Fig. 2: Forces acting on the water film

By solving Eq.(2.2), one obtains

$$u = \frac{\rho g \sin\phi}{\mu} \left[\frac{y^2}{2} - \delta y \right] + \frac{\tau_F}{\mu} y \qquad (2.3)$$

A relation between the flow rate Q and the film thickness δ can be calculated from Eq.(2.3) as

$$Q = \int_0^\delta u dy = \frac{\delta^2 \tau_F}{2\mu} \left[1 - \frac{2\rho g \sin\phi}{3\tau_F} \delta \right] \qquad (2.4)$$

So, the direction of the film flow depends on whether the parameter

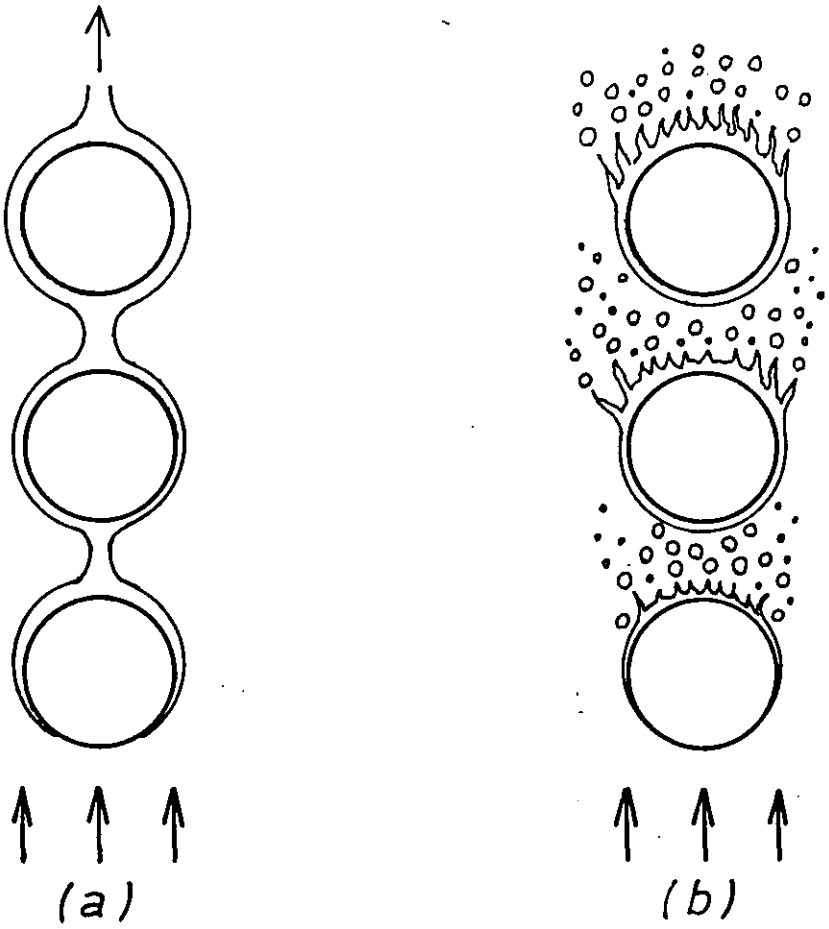

Fig. 3: Flow pattern of the water film in a rod bundle
(a) continous laminar flow,
(b) film separation and droplet formation.

$$\tau_F^* = \frac{3\tau_F}{2\rho g\delta \sin\phi} \qquad (2.5)$$

is larger than 1 or not. If τ_F^* is larger than 1, the direction will be upwards. A series of preliminary calculations indicated that τ_F^* is much larger than 1 even with $\sin\phi = 1$, except for very small gas flow rate or extremely large condensation rate.

If the gas flow rate is very low or the condensation rate is very high, δ becomes very large and thus τ_F^* becomes very small resulting in a downward film flow. Then the film will fall down and evaporate in a hotter part of the steam generator. A very complicated calculation method and long computation time will be needed to take into account the recirculation of film flow, because the downstream condition affects the upstream condition in such a case. However, this situation may take place only a limited time interval in an initial stage of accident. So, in the present calculation the film is assumed to flow upwards irrespective of the condition of τ_F^*.

Two possible patterns of the upward film flow in a tube bundle are illustrated schematically in Fig.3. In Fig.3a, the film flow is assumed to be calm and the whole flow attains to the next tube. In Fig.3b, on the other hand, the film is assumed to break into many droplets and to be dispersed into the gas flow. So, a part of the droplets will hit the next tube, while the rest will be entrained in the gas flow.

Considering the separation of boundary layer over the tube or the generation of strong eddies behind the tube, it is not realistic to imagine the calm flow such as Fig.3a takes place. Thus the flow pattern shown in Fig.3b appears to be a better assumption in the present calculation.

2.3 Entrainment

It is well known that the entrainment is observed in a film flow over a flat plate. This type of entrainment is resulted from unstable wavy motion of the film surface. The entrainment in the present situation

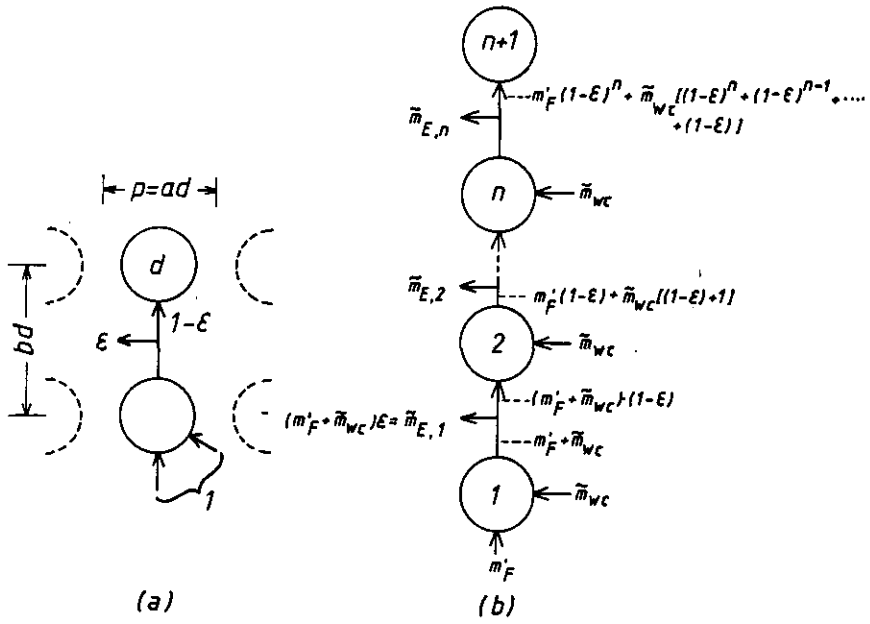

Fig. 4: Calculation model for entrainment ratio

is perfectly different from the one for the flat surface; that is, all the film is once dispersed into the gas during the transfer to the next tube. So, an amount of the entrainment will be much larger than that of the film over the flat plate.

The entrainment ratio ε is defined here as the ratio of the film flow entrained into the bulk gas to the film flow that attained the tube (see Fig.4(a)). So, the rest of the film $(1-\varepsilon)$ will attain the next tube.

If the film is dispersed uniformly into the gas, then ε is equal to $1-d/p$, where d and p are the tube diameter and the pitch, respectively. In reality, ε will be smaller than this value, because the concentration of the entrained droplets will be larger just behind the tube. However, $\varepsilon = 1-d/p$ appears to be a reasonable approximation. The effect of ε will be examined later.

Fig.4(b) shows the mass balance of the film flow and the entrainment in a row of n tubes. The inflow to the first tube is designated as m_F', and the wall condensation per a tube as $\tilde{m}_{wc}$. From a simple calculation, the inflow to the (n+1)th tube is obtained as

$$m_{(n+1)} = m_f'(1-\varepsilon)^n + m_{wc}\,[(1-\varepsilon)^n + (1-\varepsilon)^{n-1} + \cdots + (1-\varepsilon)]. \quad (2.6)$$

On the other hand, the total amount of water flowing into the row of the n tubes is

$$m_{in} = m_F' + n\cdot\tilde{m}_{wc}\ .$$

So, the amount of entrainment m_E is given as

$$m_E = m_{in} - m_{(n+1)}$$

$$= m_F'\,[1-(1-\varepsilon)^n] + n\cdot\tilde{m}_{wc}\,\left[1 - \frac{(1-\varepsilon)\{1-(1-\varepsilon)^n\}}{n\varepsilon}\right] \quad (2.7)$$

Equation (2.7) gives the entrainment m_E in one calculation mesh containing n tubes. The mass flux of the entrainment is assumed uniform in the mesh.

2.4 Direction of water droplet flow

Forces acting on an entrained water droplet in the gas flow are the gravity force (F_g) the drag force (F_D) and the force due to the bulk flow pressure gradient across the droplet (F_P). Since an upwards gas flow is assumed in the present analysis, the droplet will flow upwards only when $F_D + F_P > F_g$.

The gravity force can be expressed simply as

$$F_g = (\pi/6) d_d^3 \rho g \ ,$$

where d_d is the diameter of a droplet, ρ density, and g the gravity acceleration.

There are many theoretical and experimental works on the drag force over a sphere. According to the famous Stokes' theory, the drag force is given by "Rigid sphere"approximation as

$$F_D = 3\pi\mu u d_d \ , \qquad (2.8)$$

where μ is the viscosity of the gas. This equation is applicable only for very low Reynolds numbers. For larger Reynolds numbers, the drag force becomes larger than the value given by Eq.(2.8) owing to the separation of the boundary layer and formation of turbulent wake. So, Eq.(2.8) can be used as a lower limit of the drag force.

The force due to the pressure gradient of bulk flow can be expressed approximately as

$$F_P = \frac{dP}{dx} \cdot \frac{\pi}{4} d_d^2 \cdot d_d ,$$

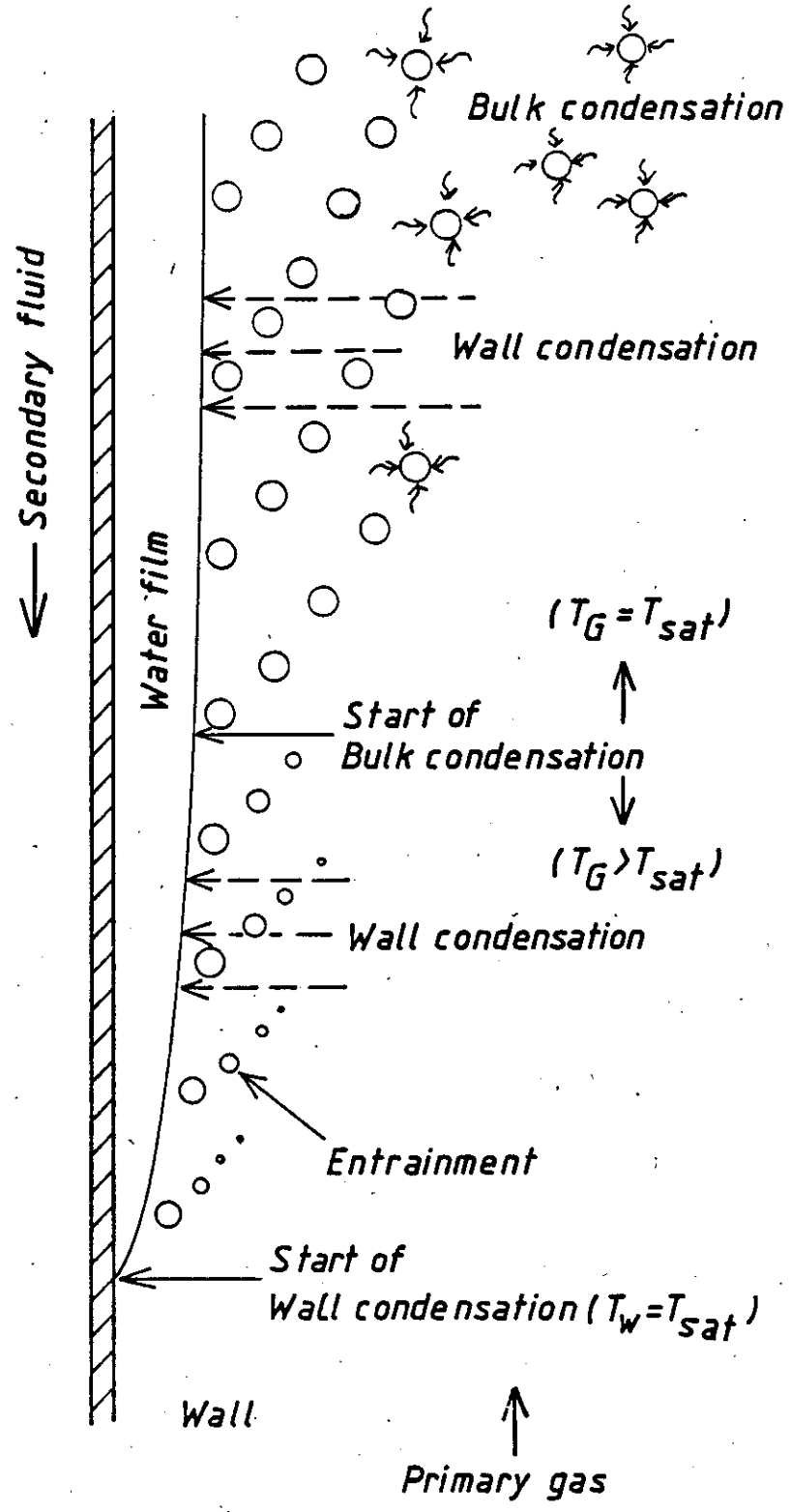

Fig. 5: Condensation model underlying the analysis

where dP/dx is the pressure gradient. If dP/dx is estimated from a correlation given in Appendix II, one can find that F_p is negligible compared to F_D.

Now let us assume that a droplet with diameter d_d is just standing ($u = 0$) in upward flow of velocity u_m. Then the forces acting upwards are F_D and F_p, and the one downward is F_g. Since $F_D >> F_p$, one determine the flow direction by calculating the following non-dimensional number:

$$F_D^* = F_D/F_g = 18\mu u_m/(\rho d_d^2 g) \tag{2.9}$$

If $F_D^* > 1$, then the water droplet will flow upward, and downward if $F_D^* < 1$.

It is difficult to estimate the diameter d_d of the entrained droplets. It seems not to be realistic to assume that the break down of the film produces a droplet with a diameter larger than the film thickness. So, if d_d in Eq.(2.9) is taken as the film thickness, it will give roughly a lower limit of F_D^*. Calculation in the present study has always shown that F_D^* defined as Eq.(2.9) is larger than 1. So, the entrained water droplet can be assumed to flow upwards accompanied by the gas flow.

In the actual numerical calculation, the rod bundle must be replaced by a continuous heat transfer surface with the same heat transfer area. So finally, the calculation model shown in Fig.5 is applied in the present analysis.

Figure 5 shows the model mentioned above schematically. Where $T_w = T_{sat}$, the wall condensation will start. The condensation rate $\dot{m}_{WC}$ is given by Eq.(2.1), and the entrainment rate m_E by Eq.(2.7). The entrained droplet will evaporate again because the bulk gas temperature does not reach the saturation temperature yet. If $T_G = T_{sat}$, the bulk condensation starts and the entrained droplets stay in the gas serving as nuclei for the bulk condensation.

2.5 Heat Transfer Coefficient

Heat removed from the gas side consists of two parts; that is, the latent heat transport accompanied by the mass transfer (q_{lat}) and the sensitive heat transport (q_{sens}). The former can be obtained from Eq.(2.1) by mutiplying the latent heat released (L_w);

$$q_{lat} = L_w \beta_{wc} (P_D - P_{D,F}) \tag{2.10}$$

The sensitive heat transport is expressed as

$$q_{sens} = \alpha_g (T_G - T_F), \tag{2.11}$$

where α_g is the heat transfer coefficient.

In case of the classical problem of the condensation for the saturated vapor, this sensitive heat transport is much smaller than the other and is neglected often. In this case, however, it is rather large because the existence of the non-condensable gas makes the temperature difference between T_G and T_F large.

The heat transfer coefficient α_g is here obtained following to Ref. (1). In this method, α_g is assumed to be the same as the one for the flow without the phase change. The heat transfer coefficient or the Nusselt number for a rod bundle placed vertically to the flow is given as

$$Nu_{bundle} = f_\psi \, Nu_0, \tag{2.12}$$

where Nu_0 is the Nusselt number for a single tube and f_ψ is a factor larger than 1 relevant to the bundle geometry. More detailed description of Nu is given in Appendix II.

It should be noted that, although the effect of the phase change on the sensitive heat transfer is neglected, an effecitve heat transfer coefficient defined as

$$\alpha_{eff} = (q_{lat} + q_{sens})/(T_G - T_w) \tag{2.13}$$

is of course increased owing to the latent heat transport compared to the sensitive heat transfer without phase change.

2.6 Shear Stress

It is assumed here again that the shear stress is not affected by the phase change. Because the condensed film over the surface is so thin (often less than 0.2 mm), this assumption appears to be reasonable. From the same reasoning, the shear stress over the film is assumed to be same as the one for a tube without film.

A relation between the shear stress τ_w and the pressure drop for one pitch of the tube is given as

$$\tau_w \pi d = \Delta P \; a \; d. \tag{2.14}$$

A correlation for the pressure drop ΔP is found in Ref.(1) for a tube bundle. Some description is given in Appendix II.

2.7 Turbulence effect in film

Reynolds number for film flow is usually defined as

$$Re_F = 4\rho\delta u/\mu \quad , \tag{2.15}$$

where ρ is the density, δ thickness, u mean velocity, and μ viscosity of the film.

According to Ref. /2/, the flow pattern of the film over a vertical wall is given as follows.

laminar flow without rippling	Re_F > 4 to 25
laminar flow with rippling	4 to 25 > Re_F > 1000 to 2000
turbulent flow	Re_F > 1000 to 2000

Some preliminary calculations have shown that typical Re_F in the present flow is roughly 50 - 200 at the outlet of steam generator depending on conditions. So, the flow cannot be a quiet laminar flow but might be the laminar flow with rippling. Moreover, the criteria above is valid for a vertical smooth wall, while the present configuration is a tube bundle. So, effects of rippling or turbulence probably start to appear already at a smaller Reynolds number. So-called effective viscosity μ_{eff} or thermal conductivity λ_{eff} are introduced to take the turbulence effect into account. Those are defined as

$$\mu_{eff} = f_{turb}\,\mu$$
$$\lambda_{eff} = f_{turb}\,\lambda, \qquad (2.16)$$

where μ and λ are the molecular viscosity and thermal conductivity of water, and f_{turb} is the turbulence factor larger than 1. This is a usual method to take into account the turbulence effect approximately.

A parametric study made later in this paper will show that the effect of f_{turb} is rather small.

3. Modelling of the steam generator

3.1 Pressure law

A relation between the total gas pressure P_G and the partial pressures P_{NC} and P_D is given as

$$P_G = P_{NC} + P_D \tag{3.1}$$

If the gas temperature is saturated, the partial pressure of the steam is governed by

$$P_D = P_{sat}(T_G) \tag{3.2}$$

3.2 State equation

The state equation for the ideal gas is assumed:

$$\rho_{NC} = P_{NC} M_{NC}/RT \tag{3.3}$$

$$\rho_D = P_D M_D/RT \tag{3.4}$$

where M and R are the mole weight (kg/kmol) and the universal gas constant (R = 8.315 kJ/kmol k), respectively.

3.3 Mass flow

Four kinds of mass flows exist in the present model; that is, the non-condensable gas (m_{NC}), steam (m_D), water droplet (m_W) and water film flow (m_F). The non-condensable gas, the steam and the water droplet flows are assumed to have the same velocity u_m; thus,

$$m_{NC} = \rho_{NC} u_m A \tag{3.5}$$

$$m_D = \rho_D u_m A \tag{3.6}$$

$$m_W = \rho_W u_m A_W \tag{3.7}$$

where A and A_W are the flow area of gas and water droplet. The flow area of water droplet and film flow is, however, neglected compared to that of the gas flow in the following calculation.

From Eqs.(3.3) to (3.6), the following important relation can be derived:

$$m_D = m_{NC}(M_D/M_{NC})(P_D/P_{NC}) \tag{3.8}$$

The mass flow rate and the partial pressure of the steam are related by this equation. If the steam pressure and the temperature are in saturation, the gas temperature T_G is also a function of m_D (or vice versa) through Eq.(3.2).

3.4 Mass balance equations

If the wall condensation takes place but the steam temperature is not saturated, the entrained water droplets will evaporate again into the bulk gas. So, the mass balance can be described as follows (see Fig.a).

$$\begin{aligned} \Delta m_D &= \Delta m_E - \Delta m_{wc} \\ \Delta m_F &= \Delta m_{wc} - \Delta m_E \\ \Delta m_{NC} &= \Delta m_W = 0 \end{aligned} \tag{3.9}$$

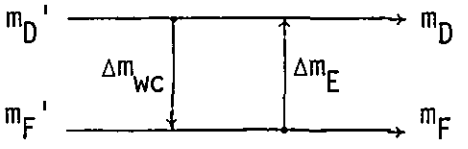

Fig. a

If the steam temperature is saturated, the entrained water will remain in form of droplets floating in the gas stream. In this case of $T_G = T_{sat}$, the bulk condensation takes place besides the wall condensation. So, the mass balance is shown in Fig. b and can be expressed as

$$\begin{aligned} \Delta m_D &= -\Delta m_B - \Delta m_{wc} \\ \Delta m_F &= \Delta m_{wc} - \Delta m_E \\ \Delta m_W &= \Delta m_B + \Delta m_E \\ \Delta m_{NC} &= 0 \end{aligned} \tag{3.10}$$

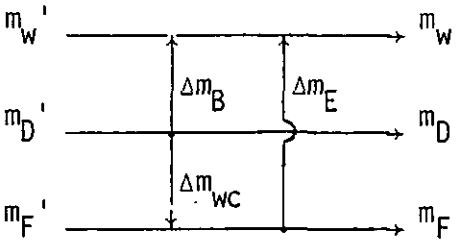

Fig. b

3.5 Energy balance equation

If the steady state is assumed, an energy balance for the primary and the secondary circuit is expressed as

$$\Delta[m_{NC}h_{NC} + m_D h_D + m_W h_W + m_F h_F] = - \Delta[m_2 h_2] \tag{3.11}$$

or

$$\Delta m_{NC}h_{NC} + m_{NC}\Delta h_{NC} + \Delta m_D h_D + m_D \Delta h_D + \Delta m_W h_W + m_W \Delta h_W + \Delta m_F h_F + m_F \Delta h_F$$

$$= - \Delta m_2 h_2 - m_2 \Delta h_2. \tag{3.12}$$

As for the sign of m's, refer to Fig.c.

The enthalpy change Δh can be related with the temperature change ΔT as follows.

$$\begin{aligned} \Delta h_{NC} &= c_{pNC}\Delta T_G \\ \Delta h_D &= c_{pD}\Delta T_G \\ \Delta h_W &= c_{pW}\Delta T_G \\ \Delta h_F &= c_{pW}\Delta T_F \end{aligned} \tag{3.13}$$

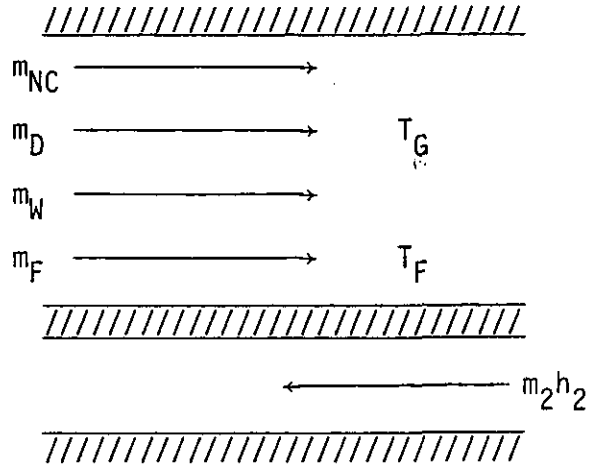

Fig. c

Thus by substituting Eqs.(3.9) and (3.10), one obtains

For $T_G > T_{sat}$;

$$(m_{NC}c_{pNC} + m_D c_{pD})\, T_G + m_F c_{pW}\Delta T_F - \Delta m_{wc}(h_D - h_F) + \Delta m_E (h_D - h_F) \tag{3.14}$$

$$= - m_2\, \Delta h_2.$$

For $T_G = T_{sat}$;

$$(m_{NC}c_{pNC}+m_Dc_{pD}+m_Wc_{pW})\Delta T_G+m_Fc_{pW}\Delta T_F-\Delta m_{wc}(h_D-h_F)+\Delta m_E(h_W-h_F)-\Delta m_B(h_D-h_W)$$

$$= - m_2\Delta h_2. \qquad (3.15)$$

Note that the multiplier if Δm_E is (h_D-h_F) in Eq.(3.14) but (h_W-h_F) in Eq.(3.15). This is because the entrained droplet evaporates in the case of Eq.(3.14) while it remains in form of droplet in Eq.(3.15).

For the enthalpy differences, the following relations exist:

$$h_D-h_F = L_w + c_{pD}(T_G-T_F)$$

$$h_W-h_F = c_{pW}(T_w-T_F) \qquad (3.16)$$

$$h_D-h_W = L_B$$

where L_W and L_B are the latent heat of phase change at the steam partial pressure on wall and in bulk gas, respectively.

So, Eqs.(3.14) and (3.15) can be further rewritten using Eq.(3.16) as

For $T_G > T_{sat}$

$$(m_{NC}c_{pNC}+m_Dc_{pD})\Delta T_G+m_Fc_{pW}\Delta T_F-\Delta m_{wc}[L_w+c_{pD}(T_G-T_F)]+\Delta m_E[L_B+c_{pW}(T_G-T_F)]$$

$$= - m_2\Delta h_2. \qquad (3.17)$$

For $T_G = T_{sat}$,

$$(m_{NC}c_{pNC}+m_Dc_{pD}+m_Wc_{pW})\Delta T_G+m_Fc_{pW}\Delta T_F-\Delta m_{wc}[L_w+c_{pD}(T_G-T_F)]+\Delta m_Ec_{pW}(T_G-T_F)$$

$$- \Delta m_BL_B = - m_2\Delta h_2, \qquad (3.18)$$

It should be noted in these equations that some of the heat are released in (or derived from) the bulk gas while the others in the wall film. The terms underlined with the solid line represent the former while the ones by the broken line the latter. This distinction is important because only the heat released in (or derived from) the bulk gas should be included in the equation of heat transfer between the bulk gas and the film.

3.6 Heat Transfer equation

(a) Heat transfer between the bulk gas and the wall film

Referring to Eqs.(3.17) and (3.18), one obtains the equation for the heat transfer between the gas and the wall film.

$$(m_{NC}c_{pNC}+m_{D}c_{pD}+m_{W}c_{pW})\Delta T_G/\Delta F-\dot{m}_{wc}c_{pD}(T_G-T_F)+\dot{m}_{E}c_{pW}(T_G-T_F)$$

$$\underbrace{+\dot{m}_{E}L_{B}}_{(a)}\underbrace{-\dot{m}_{B}L_{B}}_{(b)} = -\alpha_1(T_G-T_F), \qquad (3.19)$$

where $\dot{m}=\Delta m/\Delta F$ and α_1 is the heat transfer coefficient given by Eq.(2.11). The term (a) is zero if $T_G = T_{sat}$, while the term (b) is zero if $T_G>T_{sat}$ (see Eqs.(3.17) and (3.18)).

Equation (3.19) can be rewritten as

$$(\overline{mc_p})_1(dT_G/dF) = -\alpha^*(T_G-T_F) - (\dot{m}L)^*, \qquad (3.20)$$

where

$$(\overline{mc_p})_1 = m_{NC}c_{pNC} + m_{D}c_{pD} + m_{W}c_{pW}$$

$$\alpha^* = \alpha_1 + \dot{m}_{E}c_{pW} - \dot{m}_{wc}c_{pD} \qquad (3.21)$$

$$(\dot{m}L)^* = \dot{m}_{E}L_{B} - \dot{m}_{B}L_{B}$$

Eqn. (3.20) may be integrated for an increment $\Delta F = F_i - F_{i-1}$ of the primary heat exchanging area which is limited in such a manner that α^* can be regarded as practically constant within its boundaries. If one assumes that the film temperature T_F varies linearely within this increment (see Fig. d) then the following solution will be obtained for a given $T_{F,i}$:

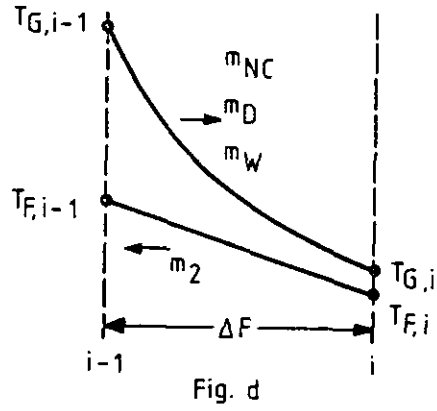

Fig. d

$$T_{G,i} = T_{G,i-1} - [(T_G - T_F)_{i-1} + (mL)^*/a^*] (1-e^{-x^*}) - (T_{F,i-1} - T_{F,i}) [1 - (1-e^{-x^*})/x^*] \quad , \tag{3.22}$$

where $x^* = \alpha^* \Delta F / (\overline{mc_p})_1$.

(b) Heat transfer to the primary wall

Heat transfer to the primary wall consists of two contributions. One is the heat released in the bulk gas $Q_B = q_B \Delta F$ and the other contribution is the heat released in the film $Q_F = q_F \Delta F$. The heat flux density q_1 to the primary wall, therefore, is given by

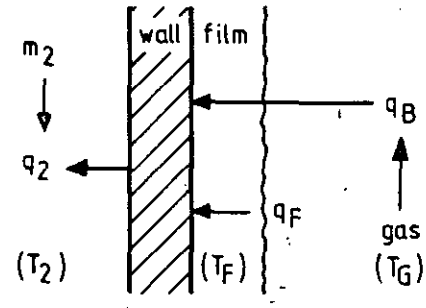

Fig. e

$$q_1 = q_B + q_F \quad , \tag{3.23}$$

where

$$q_B = \alpha_1 (T_G - T_F) . \tag{3.24}$$

The heat flux density q_F consists of two parts

$$q_f = m_{wc} L_w - m_F c_{pw} \Delta T_F / \Delta F \quad . \tag{3.25}$$

The first term in this equation represents the heat released over the film due to wall condensation, and the last term corresponds to the convection of the film flow. In the following the difference between the surface and the average temperature of the film will be neglected because this difference is small compared to the total temperature difference between the wall and the bulk fluid in the primary channel.

Heat flux to the secondary fluid is given as

$$q_2 = \alpha_{eff2}(T_F - T_2), \tag{3.25}$$

where α_{eff2} is the effective heat transfer coefficient between the film and the secondary fluid:

$$1/\alpha_{eff2} = \delta_F/\lambda_F + d_w/\lambda_w + 1/\alpha_2. \tag{3.26}$$

This heat flux q_2 must be equal to a sum of $q_B + q_F$; that is,

$$q_2 = q_B + q_F \tag{3.27}$$

The film temperature $T_{F,i}$ for which this equation is satisfied will be determined by iteration within the solution procedure as described in section 4.

3.7 Heat transfer and energy balance equation for the secondary circuit

The heat transfer coefficient for the secondary circuit α_2 is given by usual correlation for forced convection heat transfer with and without phase change.

Energy equation for the secondary circuit can be written as

$$m_2 c_2 (dT_2/dF) = -q_2 \tag{3.28}$$

where q_2 and m_2 are positive for the direction shown in Fig.e and Fig.d. The specific heat capacity c_2 is given as

$c_2 = c_{pW}$ for water cooling region

$c_2 = \infty$ for evaporation region

$c_2 = c_{pD}$ for steam cooling region

This means that in the evaporation region the secondary fluid temperature is assumed to be constant at the saturation temperature.

For a finite increment ΔF of heat exchanging area, Eq.(3.28) can be simply integrated as

$$T_{2,i} = T_{2,i-1} - q_2 \Delta F/(m_2 c_2) \tag{3.29}$$

3.8 Heat transfer without condensation

If no condensation takes place, the heat transfer between the primary gas and the secondary water/steam can be given as

$$(m_{NC}c_{pNC}+m_D c_{pD})(dT_G/dF) = - \alpha_{eff}(T_G-T_2) \tag{3.30}$$

$$m_2 c_2 (dT_2/dF) = - \alpha_{eff}(T_G-T_2) \tag{3.31}$$

where

$$1/\alpha_{eff} = 1/\alpha_1+d_w/\lambda_w+1/\alpha_2. \tag{3.32}$$

this treatment is possible only when q_F in Fig.e is zero.

From Eqs.(3.28) and (3.29), one obtains

$$d(T_G-T_2)/dz = -(T_G-T_2) \tag{3.33}$$

where

$$z = \alpha_{eff}(-1/m_2 c_2+1/(m_{NC}c_{pNC}+m_D c_{pD}))F, \tag{3.34}$$

This differential equation can easily be integrated as

$$(T_G-T_2)_i = (T_G-T_2)_{i-1} e^{-\Delta z} \tag{3.35}$$

On the other hand, Eqs.(3.30) and (3.31) give

$$T_{2,i} = T_{2,i-1} + \frac{m_{NC}c_{pNC}+m_D c_{pD}}{m_2 c_2}(T_{G,i}-T_{G,i-1}) \tag{3.36}$$

By substituting Eq.(3.36) into (3.35), one can get the following equation.

$$T_{G,i} = T_{G,i-1} - (T_G-T_2)_{i-1} \frac{(1-e^{-\Delta z})}{1-(m_{NC}c_{pNC}+m_D c_{pD})/m_2 c_2} \qquad (3.37)$$

This equation together with Eq.(3.36) gives the variation of T_G and T_2 in ΔF for the case of no condensation.

3.9 Outlet mixing calculation

At the outlet of the primary fluid, the following components exist.

	Mass flow rate	temperature
Non-condensable gas	m_{NC}	T_G
Steam	m_D	T_G
Water droplets	m_W	T_G
Water film	m_F	T_F

Depending on the outlet conditions, not all of these components are always existing.

The film temperature T_F is always lower than that of the other components. So, if all the components are mixed, a new equilibrium temperature will be reached. When the film flow is mixed with the bulk temperature T_G will decrease and some part of the steam will condense forming water droplets. This heat and mass balance calculation is made with the assumption of equilibrium state for the phase change. This calculation is called below as "Outlet mixing".

In some calculations, to examine an effect of the condensation, the occurrence of the condensation is suppressed artificially even if $T_G < T_{sat}$. In this case, there are always only two components m_{NC} and m_D at the outlet. The gas temperature is of course subcooled. Then, the outlet mixing calculation is made to bring this inequilibrium state into the equilibrium one. That is, a part of the steam is condensed

at first. Then, the saturation temperature corresponding to the steam pressure decreases, while the gas temperature increases owing to the latent heat released by the condensation. An iterative procedure will be continued until the saturation and the gas temperatures become equal. Thus, a new equilibrium state can be obtained, where m_{NC}, m_D, and also m_W are now existing.

4. Evaluation method

The model which has been described in the previous sections has been applied to a typical HTR steam generator with countercurrent flow. The heat exchanging area is subdivided into a certain number of equally spaced discretization intervals. The integration of the governing equations is started in the inlet plane of the primary gas flow. Since this plane is the outlet of the secondary flow, the integration proceeds opposite to the secondary flow direction. The integration procedure starts with some initial guess of the secondary outlet enthalpy. If the secondary enthalpy at the end of the integration does not agree with the specified inlet enthalpy, an iteration routine will be initiated which modifies the outlet enthalpy and repeats the calculation procedure until agreement with the specified inlet enthalpy is attained within a certain error tolerance.

The computing program checks in every integration step the flow conditions on the primary and secondary side and assigns the proper parameters, heat transfer coefficients and condensation conditions to the subinterval being treated. The integration in direction of the primary flow has the advantage that the onset of film and bulk condensation can easily be identified.

The evaluation procedure consists of the following steps:

(1) Specify inlet conditions of the primary and secondary flow,

(2) specify a first guess for the outlet enthalpy of the secondary fluid,

(3) integrate, using Eqns. (3.38) and (3.39), up to the point where wall condensation starts,

(4) specify a first guess for the film temperature $T_{F,i}$ and iterate until Eqn. (3.42) is satisfied,

(5) continue this procedure up to the point where bulk condensation starts,

(6) specify a first guess for the film temperature $T_{F,i}$,

(7) specify a first guess for the bulk condensation rate m_B and iterate until Eqn (3.43) is satisfied,

(8) go back to (7) and iterate until Eqn. (3.42) is satisfied,

(9) continue this calculation up to the outlet of the primary gas,

(10) compare the obtained enthalpy of the secondary fluid with the specified inlet value,

(11) go back to (3) and iterate until the obtained and the specified inlet enthalpy of the secondary fluid agree,

(12) perform the outlet mixing calculation to bring the primary gas-water mixture into an equilibrium state.

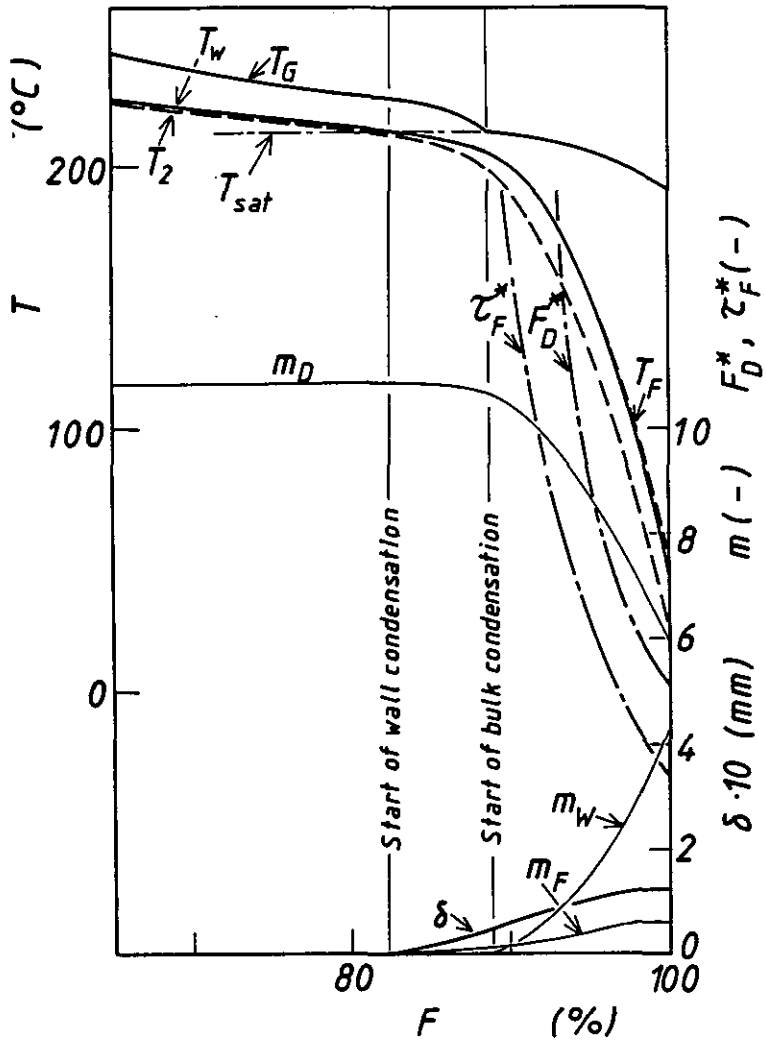

Fig. 6: Typical results in the heat exchanging region with condensation on the primary side

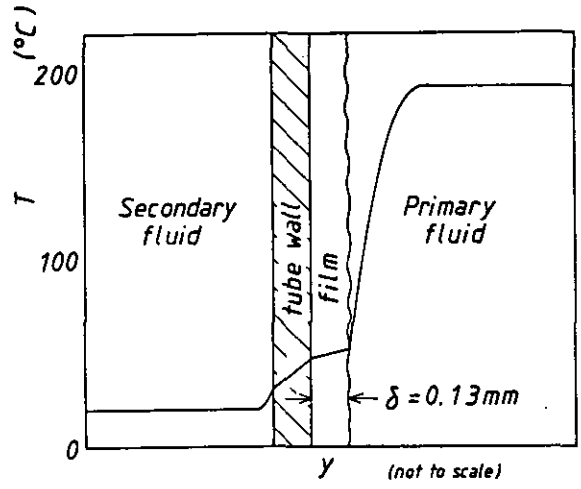

Fig. 7: Relative importance of thermal resistances

5. Results

5.1 Typical example

A typical result is shown in Fig. 6. The horizontal axis F is the relative heat transfer area in the steam generator. 100% corresponds to the outlet of the primary gas. The flow direction of the primary helium/steam mixture is from F = 0 to 100%, while the secondary water/steam flows in the opposite direction.

Input conditions are

Primary side

Inlet temperature	$T_{G,in}$ = 400°C
Total pressure	P_G = 5.5 MPa
Pressure of non-condensable gas	P_{NC} = 3.5 MPa
Inlet pressure of steam	$P_{D,in}$ = 2.0 MPa
Mass flow rate	m_1 = 20 kg/s

Secondary side

Inlet temperature	$T_{2,in}$ = 20°C
Pressure	P_2 = 6.5 MPa
Mass flow rate	m_2 = 20 kg/s

Geometrical data are similar to the design of THTR.

The wall condensation starts at the point where the wall temperature T_W falls down to the line of the saturation temperature T_{sat}. The film thickness δ and the film flow rate m_F start to increase from this point. The water droplet flow rate m_W remains still to be zero at this point. This is because the bulk condensation does not start yet and also because the entrained droplet is assumed to evaporate immediately.

The bulk condensation starts where the bulk gas temperature T_G decreases down to the saturation temperature. At this point, the bulk gas temperature T_G abruptly changes its gradient to be small. This is because the latent heat of condensation is released in the bulk gas and thus it seems as if the effective heat capacity is increased.

After the start point of the bulk condensation, the water droplet flow rate m_W starts to increase and the steam mass flow rate m_D to decrease remarkably.

The two non-dimensional parameters τ_F^* and F_D^* defined by Eqs.(2.5) and (2.9) are also given in Fig. 6. Both of the parameters are essentially larger than unity; so the present assumption of upwards flow for the film and the droplet appears to be valid.

At the outlet of the steam generator (F = 100%), the film thickness δ is 0.13 mm. This fairly small thickness is not surprising; It is typical of the film condensation. Moreover, the entrainment of the film also tends to make the film thinner.

The temperature distribution parpendicular to the flow is shown schematically in Fig.7. The horizontal axis is the distance from the tube wall, but it is not drawn to scale. One can clearly see that the main thermal resistance lays in the primary gas mixture of steam and non-condensable gas. The thermal resistance in the film is so small that no detailed study is required for the heat transfer coefficient of the film flow.

Values of the empirical parameters used in this example are $\varepsilon = 0.3$ and $f_{turb} = 20$. Effects of these parameters are discussed below.

5.2 Empirical parameters

A parametric study has been made to study the effects of the empirical parameters ε and f_{turb} and the number of nodes N. Results obtained are given in Table 1. The inputs not designated in the Table are the same as those for Fig. 6. The parameters, ε and f_{turb}, have fairly large effect on the film thickness; but they have no large effect on the outlet gas temperature (T_G) or steam pressure (P_D). The transferred energy (Q_{tr}) is also not affected by the ε or f_{turb} assumed here. This is because the thermal resistance of the film is of less importance compared to that of the primary gas as discussed above. So, the selection of these values has no large effect on the final results.

In the following calculations,

$$\varepsilon = 0.3 \text{ and } f_{turb} = 20.$$

will be used. The value of ε is obtained from geometrical considerations ($\varepsilon \sim 1 - p/d$) as discussed before. The value of f_{turb} is typical for turbulent flow at low Reynolds number.

The effect of node numbers (N) has also been examined. No large effect on the computed results is found in the range of N = 30 - 200 (see Table 1). So, N = 60 has been used in the following to save computation time.

In case 10 of Table 1, the condensation is artificially suppressed; so the outlet temperature of steam generator (S.G.) is largely subcooled. After the "outlet mixing", this subcooled gas is brought into an equilibrium condition. One can see the effect of the condensation clearly by comparing the numbers in the column of the "transferred heat" Q_{tr}. The transferred heat Q_{tr} is increased about 20% in this example by taking the condensation into account. The effect of condensation is discussed further in the following chapter.

5.3 Effect of condensation

Results of calculations with and without the condensation are compared in Fig.8. Conditions of the calculation are the same for the both cases. The broken line refers to the condensation artificially suppressed.

As the condensation is suppressed in the calculation "without condensation" (broken line), the gas temperature T_G is largely subcooled at the outlet (F = 100%). This nonequilibrium condition is brougt into equilibrium by "outlet mixing". Here, a part of the steam is condensed releasing its latent heat. So the saturation temperature T_{sat} decreases while the gas temperature T_G increases. A new equilibrium is reached when $T_G = T_{sat}$ is attained. Thus, in the case of the broken line,

T_G is raised due to "outlet mixing".

The solid line shows a result of calculation with condensation. "w.c." and "b.c." indicate the start point of wall and bulk condensation respectively. In the "outlet mixing" procedure, the bulk gas is mixed with the film water flow to thermal equilibrium. Since the film temperature T_F is lower than the gas temperature, T_G decreases slightly due to outlet mixing.

If the gas temperatures T_G of both calculations are compared at the outlet of the steam generator (F = 100%), the differece is found to be fairly large. This is because T_G of the broken line is in a nonequilibrium condition. After the "outlet mixing", however, the difference is very small. The difference in the transferred heat Q_{tr} is only 3% in this example.

One may expect that the condensation will increase the heat transfer owing to the latent heat transport. Nevertheless, the total heat transferred Q_{tr} is nearly the same for the both cases. The reason is discussed below.

The heat flux from the primary to secondary fluid (q) is compared in Fig.8. The heat flux q of the solid line increases remarkably in the region where condensation takes place. This is of course due to the contribution of the latent heat transport. Owing to this enhanced heat transfer, the secondary fluid temperature T_2 increases steeply in this region. (Note that the secondary fluid flows from F = 100 to 0 in this figure.) So, the temperature difference between T_G and T_2, and thus the heat flux q, become smaller in the rest part of the area. This effect compensates the enhanced heat transport by the condensation.

With the assumption of no condensation, however, the temperature difference between T_G and T_2 is kept to be relatively large in whole of the heat transfer area. Thus the heat flux q also remains to be an appreciable value in the whole area. So, the transferred heat is not decreased so much even if the condensation is suppressed. This is the reason why the condensation does not increase the transferred heat Q_{tr}.

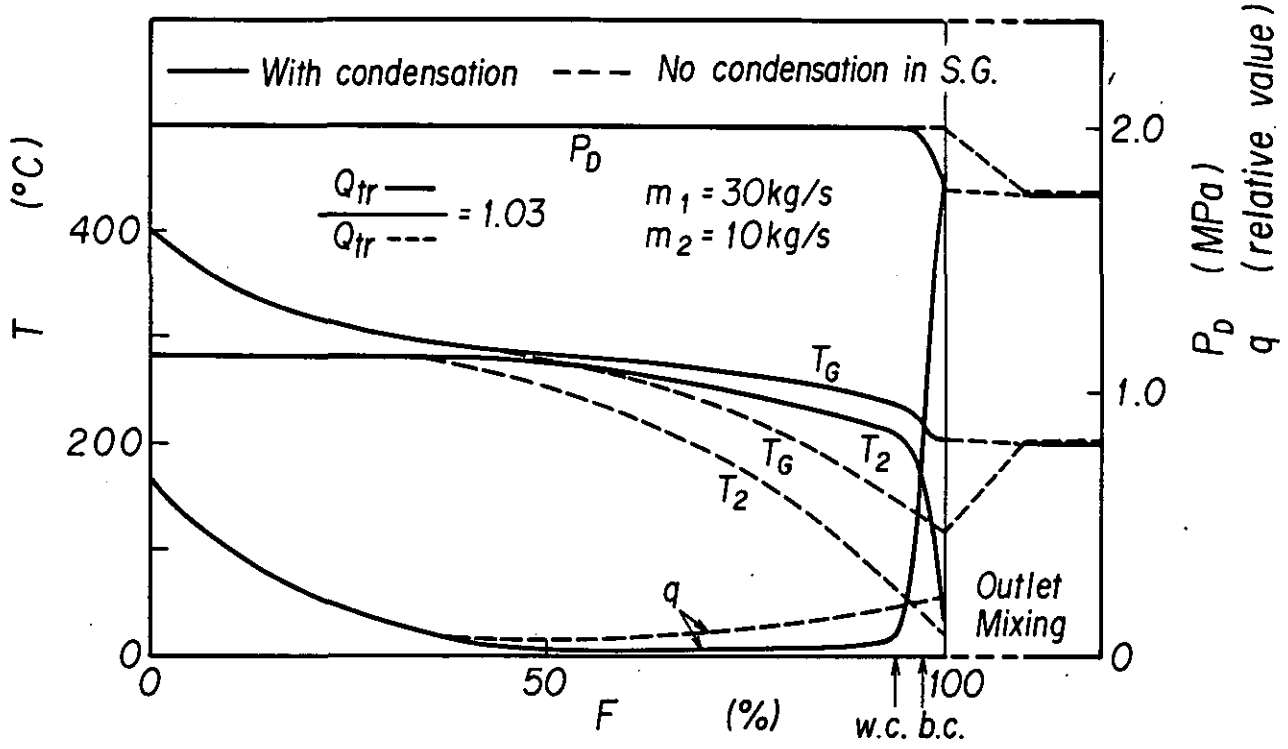

Fig. 8: Comparison of results with and without condensation. Example 1

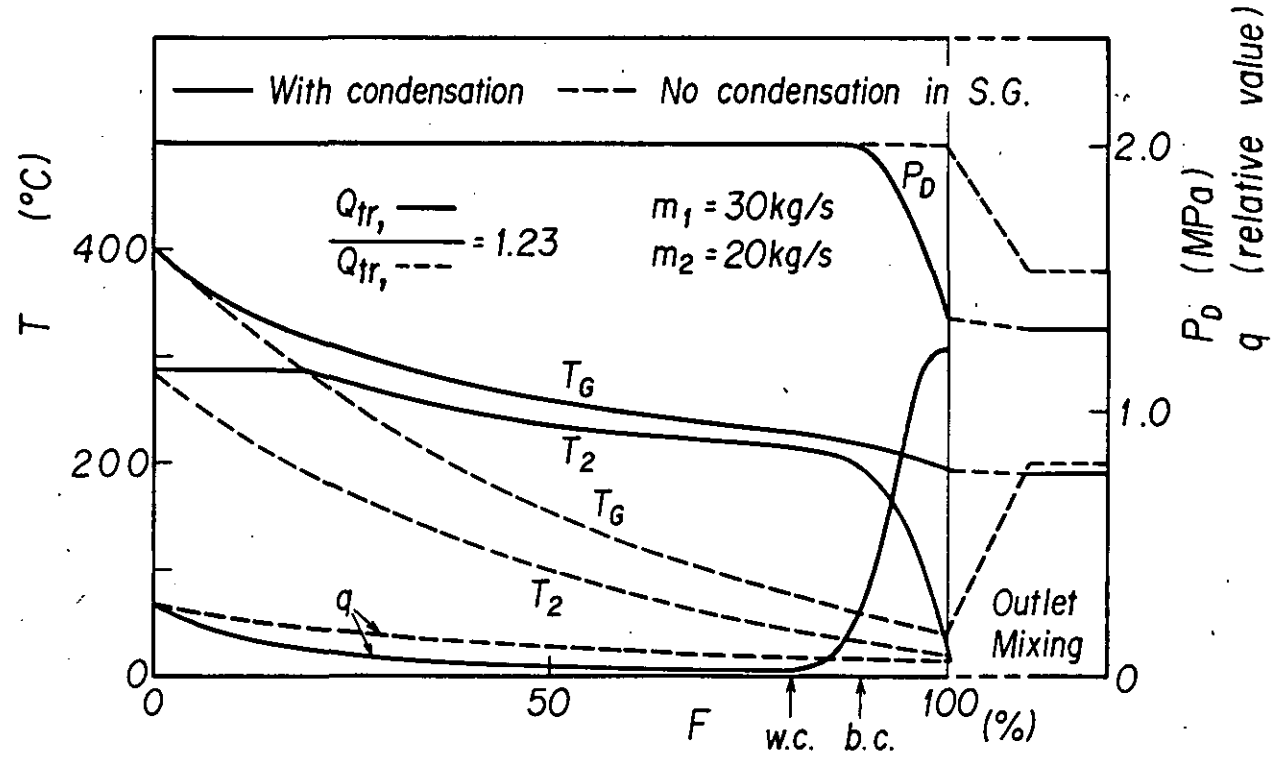

Fig. 9: Comparison of results with and without condensation. Example 2

From the reasoning above, it is expected that the effect of condensation is more evident if the secondary mass flow rate m_2 is increased. As the rise of T_2 is smaller for a larger m_2, a larger temperature difference will be kept between T_G and T_2 if m_2 is increased.

In Fig.9, the secondary mass flow rate m_2 is doubled. In this case, the difference between the solid and broken lines is remarkable even after the outlet mixing. The transferred heat is increased more than 20% by the condensation. So, one can conclude that neglecting the condensation effect results in a larger error for a larger m_2.

The effect of the secondary mass flow rate m_2 is further studied in Fig.10. Calculations for three different values of m_2 are compared in this figure. One can see that the area where the condensation takes place increases with increase of m_2. It is interesting to note that, even for a very high flow rate of m_2 = 30 kg/s, the condensation takes place only in less than one third of the total area.

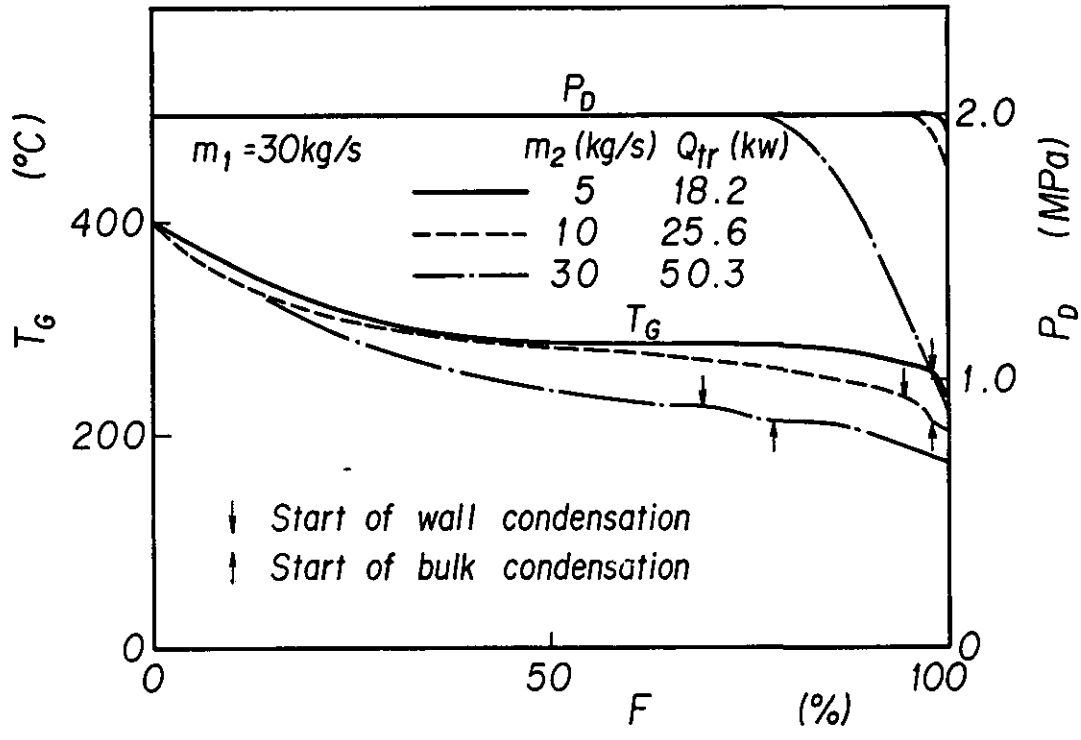

Fig. 10: Effect of the secondary mass flow rate

Case	Inlet Condition			Empirical Parameter			Outlet of S.G.			After mixing		
	T_{Gin}	T_{2in}	P_{Din}	ε	f_{turb}	N	T_G	P_D	δ	T_G	P_D	Q_{tr}
	°C	°C	MPa				°C	MPa	mm	°C	MPa	kW
1	400	20	2.0	0.3	10	60	192.5	1.326	0.134	191.6	1.301	38.6
2	*	*	*	0.0	*	*	196.5	1.446	0.335	191.5	1.300	38.6
3	*	*	*	0.5	*	*	192.0	1.314	0.087	191.6	1.303	38.5
4	*	*	*	0.75	*	*	191.8	1.307	0.050	191.7	1.303	38.5
5	*	*	*	*	20	*	192.5	1.328	0.190	191.6	1.303	38.5
6	*	*	*	*	1	*	192.4	1.324	0.042	192.6	1.301	38.5
7	*	*	*	*	*	30	193.1	1.343	0.128	192.1	1.317	38.5
8	*	*	*	*	*	100	192.4	1.323	0.135	191.5	1.299	38.6
9	*	*	*	*	*	200	192.3	1.326	0.136	191.4	1.300	38.6
10	*	*	*	No condensation		*	40.2	2.000	0.0	198.8	1.517	31.4

* indicates the same figure as Case 1.

Table 1 Effect of empirical parameters and number of nodes

6. A program module based on a simplified condensation model

The program described in the previous sections has been used as a subroutine in the computer program COROX which has been developed to simulate the dynamic behaviour of the primary system of an high temperature reactor in case of a water ingress accident. Experience, however, showed that computing time requirements were unsatisfactorily high. The COROX-code, when used to analyse long term transients may call the steam generator routine several hundred times per run. Computing economy, therefore, becomes important.

The computing time requirement of the code described before is essentially due to the large number of discretization intervals needed for a detailed representation of the temperature distribution in both flow channels and by the nested iterations in the region of primary condensation. In a program which simulates the total primary circuit, however, these distributions are normally not required. The interesting quantities which should be supplied by the steam generator routine in this case are the primary outlet temperature, the primary condenswater flow and the power transferred to the secondary side.

A program module, therefore, has been developed which has been designed to minimum computing time requirements. This has been achieved by minimizing the number of intervals of the heat exchanging area over which the steam generator equations are integrated in one step. In addition some simplifications have been included which have been suggested by the detailed investigation described before. These simplifications may, in some cases, cause a certain loss of accuracy but it will be shown that deviations are in general small enough to be acceptable.

A variable boundary technique has been used to minimize the number of integration intervals. The total heat exchanging area of the steam generator is divided into three parts as shown in Fig. 11. They correspond to the subcooled region, the evaporation region and the steam superheating region on the secondary side. The location of these boundaries are determined by the saturation enthalpies of water and steam corresponding to the pressure on the secondary side. Therefore, they depend on boundary conditions. One or both boundaries may be missing under certain inlet conditions. The

formalism to determine the location of these boundaries is derived in Ref. /4/. The subdivion of the evaporation region into a nuceate boiling region and a region with film boiling heat transfer is a special feature of the steam generator model of Ref. /4/ and is not used in the comparative calculations presented below.

To include primary condensation an additional division of the subcooled region into three subregions is introduced to which different conditions on the primary side are assigned. The first region is characterized by simultaneous wall and bulk condensation (condensation region II), the next subregion by wall condensation only (condensation region I) and the third subregion by the absence of condensation. We note that condensation on the primary side is considered only in the subcooled region of the secondary side.

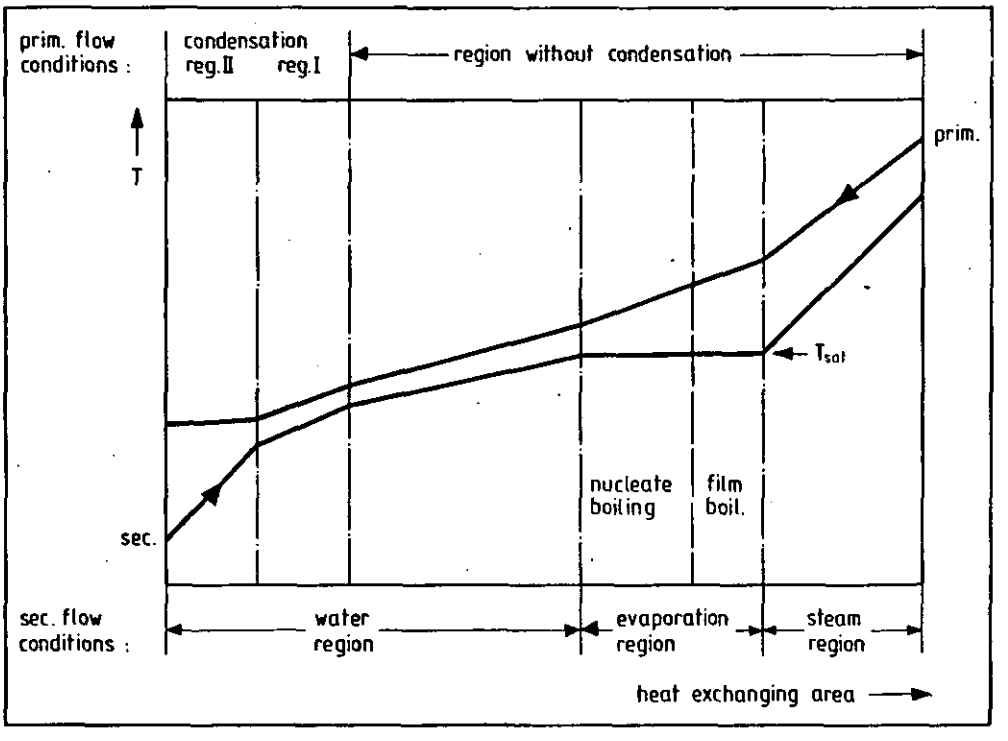

Fig. 11: Scheme of variable boundary steam generator model

The location of the boundary between the condensation region I and the region without condensation is given by the point where the primary wall temperature attains the saturation temperature related to the inlet steam partial pressure. The boundary between condensation regions I and II is determined by the point where the primary bulk fluid temperature attains the saturation termperature according to the local steam partial pressure. The determination of the locations of these boundaries requires, if an iterative solution procedure shall be avoided, transformation of the equations governing primary condensation to a form which formally corresponds to the equation without condensation. To be able to integrate the steam generator equations over both condensation regions in one step it is necessary to introduce certain simplifications of the model. These modifications will be explained below.

6.1 Mass balance in the range of condensation

To treat the regions with condensation on the primary side, the following simplifying assumptions are made:

The thickness of the condensate film on the surface of the heat exchanging tubes is constant in time under otherwise steady state conditions. This means that no net water mass transfer exists between the bulk and the film: the water formation on the wall is compensated by entrainment in form of droplets to the bulk flow. Since, in addition, the film mass flow remains small compared with the total mass flow, the splitting of the water flow into a droplet flow and a film flow will be abandoned.

The total water mass flow, therefore, will be approximated in the form

$$m_{H_2O} = m_D + m_W \tag{6.1}$$

where m_W is the mass flow of water in condensed form (droplets and film). The total water flow (liquid and steam) is constant and equal to the value at the inlet of the primary channel. For the primary enthalpy flow

we assume that all components of the flow have the same temperature. The total enthalpy flow on the primary side, therefore, is approximated by

$$[m_{NC}\, c_{pNC} + m_D\, c_{pD} + m_W\, c_{pW}]\, T_G = [m_{NC}\, c_{pNC} + m_{H_2O}\, c_{pW} + m_D\, (c_{pD} - c_{pW})]\, T_G \quad . \tag{6.2}$$

6.2 Heat transfer with condensation

In both condensation regions release of latent heat in the water film has to be taken into account because it forms an essential contribution to the heat transfer. Release of latent heat in the bulk fluid is taken into account only in the condensation region II.

The heat transfer to the wall across the condensate film is determined by the sensitive heat transferred from the gas to the film and the latent heat deposited in the film. The total heat flux density, therfore, is given by

$$q_1 = q_{lat} + q_{sens} \quad , \tag{6.3}$$

where both contributions are given by Eqns. (2.10) and (2.11). By introducing the ratio $\varkappa$ of the mass and heat transfer coefficient

$$\varkappa = \beta_{wc}/\alpha_g \quad , \tag{6.4}$$

Eqn. (6.3) may be written in the form

$$q_1 = \alpha_g\, [(T_G - T_F) + \varkappa\, L_W\, (p_D - p_{D,F})] \quad . \tag{6.5}$$

The difference of steam partial pressures appearing in this equation may be replaced by a corresponding temperature difference in the form

$$p_D - p_{D,F} = \frac{\Delta p_D}{\Delta T_{sat}\,(p_D)}\, (T_G - T_F) \quad . \tag{6.6}$$

The difference quotient in (6.6) may be evaluated from a suitable pair of pressures and associated saturation temperatures. Because the film surface temperature is not known in advance it is evaluated using the wall temperature as an approximation for T_F. Thus the following expression for the total heat flux density is obtained

$$q_1 = \alpha_{F2} (T_G - T_F) \tag{6.7}$$

with

$$\alpha_{F2} = \alpha_g \left[1 + \varkappa L_w \frac{\Delta p_D}{\Delta T_{sat} (p_D)}\right] \quad . \tag{6.8}$$

The heat flux may be related to the difference between wall and bulk gas temperature by introducing the film heat transfer coefficient

$$\alpha_F = \lambda_w/\delta_F \quad , \tag{6.9}$$

where δ_F is the thickness of the condensate film.

From

$$q_1 = \alpha_F (T_F - T_W) \tag{6.10}$$

one obtains

$$q_1 = \alpha_{eff} (T_G - T_W) \tag{6.11}$$

if α_{eff} is given by

$$1/\alpha_{eff} = 1/\alpha_F + 1/\alpha_{F2} \quad . \tag{6.12}$$

In the condensation region I a different situation exists because the bulk gas temperature is not in equilibrium with the steam partial pressure. The local heat transfer is given by Eqn. (6.5) at the boundary only, which this region has in common with the condensation region II. On the

other boundary (to the region without condensation), the latent heat contribution vanishes. In the condensation region I, therefore, the heat transfer coefficient α_{F2}, defined by Eqn. (6.7), varies from the value given by Eqn. (6.8) on one boundary to α_g at the other boundary. The integration of the energy equation over the condensation region I is performed with the arithmetic mean of the two boundary values taken as an average value for the heat transfer coefficient in this region.

6.3 Release of latent heat in the bulk condensation region

In the condensation region II, Eqn. (3.20) is used with the entrainment flow m_B neglegted:

$$(\overline{mc_p})_1 \, (dT_G/dF) + L_B \, (dm_D/dF) = q_1 \, , \tag{6.13}$$

with $(\overline{mc_p})_1$ given by Eqn. (3.21).

The second term on the left side of this equation represents the release of latent heat to the bulk flow. Bearing in mind that the change of the steam mass flow is assumed to be in accordance with thermal equilibrium, i.e. $T_G = T_{sat}(p_D)$, the program module uses the balance equation (6.13) transformed as follows:
The derivative of m_D appearing in Eqn. (6.13) may be written

$$dm_D/dF = (dm_D/dp_D) \cdot (dp_D/dT)_{sat} \cdot (dT_G/dF) \tag{6.14}$$

where the second factor on the right side of this equation is a derivative along the saturation line. From Eqn. (3.8) one obtains

$$dm_D/dp_D = m_{NC}(M_D/M_{NC}) \, p_G/(p_G - p_D)^2 \tag{6.15}$$

which, when inserted in Eqn. (6.13) gives

$$(mc_p)^* \, (dT_G/dF) = q_1 \tag{6.16}$$

with

$$(mc_p)^* = (\overline{mc_p})_1 + m_{NC}(M_D/M_{NC})\ (p_G/(p_G - p_D)^2) \cdot (dp_D/dT)_{sat} \cdot L_B \qquad (6.17)$$

Eqn. (6.16) is a formal reduction of (6.13) to the form derived for the enthalpy flow without condensation. It must be kept in mind, however, that T_G in this equation is supposed to be equal to the saturation temperature corresponding to the local steam partial pressure.

In the numerical treatment of the bulk condensation region an average value of $(mc_p)^*$ is assigned to this region which is chosen in the following manner:
The derivative $(dp_D/dT)_{sat}$ is replaced by the difference quotient

$$\frac{p_{Dout} - p_{Din}}{T_{sat}(p_{Dout}) - T_{sat}(p_{Din})} \qquad (6.18)$$

where p_{Dout} and p_{Din} are the outlet and inlet steam partial pressures respectively. For p_D appearing in Eqn. (6.17) a weighted average of the inlet and outlet values is used

$$p_D = \gamma \cdot p_{Din} + (1 - \gamma)\ p_{Dout} \qquad (6.19)$$

The weight factor γ has been determined by comparison with results of the detailed program described in section 3 for the same boundary conditions. Optimal agreement was obtained with $\gamma = 0{,}6$.

6.4 Determination of interval boundaries

The interval boundaries determined by the flow condition on the secondary side may be obtained by solving Eqn. (3.37) explicitely for ΔF as follows:

$$\Delta F = -\frac{1}{\omega} \ln \left[1 - \frac{(h_{n,i} - h_{2,i-1})\ m_2\omega}{\alpha_{eff}\ (T_{G,i-1} - T_{2,i-1})}\right] \qquad (6.20)$$

with

$$\omega = \alpha_{eff}\ [-1/m_2c_2) + 1/(m_{NC}\ c_{pNC} + m_D\ c_{pD})] \qquad (6.21)$$

where the secondary temperature difference has been replaced by the corresponding enthalpy difference.

If h_{2i} is a specified enthalpy then ΔF from Eqn. (6.20) is the area increment necessary to advance the enthalpy from h_{2i-1} to h_{2i}. If h_{2i} and h_{2i-1} are enthalpies either representing region boundaries or the inlet or outlet plane, then this equation can be used to determine the extent of the subcooled, the evaporation and the steam superheating region.

The primary gas temperature at these region boundaries can be calculated from the energy balance Eqn. (3.36) if the boundary is outside of the region of primary bulk condensation.

The same formalism can be used to determine the locations of the boundaries of the condensation regions on the primary side if the energy balances are used which have been transformed to the same type of equations which govern the regions without condensation.

If a bulk condensation region exists then its boundary on one side will be the plane of the secondary inlet and the boundary on the other side that to the condensation region I (see Fig. 11). The area occupied by this region may be evaluated from Eqn. (6.20) with

$$h_{2,i-1} = h_{2in} \quad \text{and} \quad h_{2,i} = h_{2B} ,$$

where h_{2in} is the secondary inlet enthalpy and h_{2B} the secondary enthalpy at the other boundary.ω has to be evaluated using Eqn. (6.21) with $m_{NC}\, c_{pNC} + m_D\, c_{pD}$ replaced by $(mc_p)^*$ according to Eqn. (6.17) and α_{eff} given by Eqn. (6.12).

The enthalpy h_{2B} has to be calculated from the energy balance (3.36) with $T_{G,i}$ equal to the saturation temperature corresponding to the steam partial pressure p_{D1} at the location of the boundary:

$$h_{2B} = h_{2in} - (mc_p)^* \, (T_{sat}(p_{D1}) - T_{Gout})/m_2 . \qquad (6.22)$$

Since the loss of steam in the bulk due to film formation is neglected in condensation region I, p_{D1} may be set equal to the inlet steam partial pressure. We note that the assumption of thermal equilibrium in this region implies that

$$T_{Gout} = T_{sat}(p_{Dout}) \; . \tag{6.23}$$

If this condensation region exists, it follows that the outlet steam partial pressure p_{Dout} must be smaller then the inlet value p_{Din}.

If the condensation region I exists, two cases have to be considered: If the condensation region II also exists, then the boundary which is common to both regions lies inside the primary channel. If this is not true, the left boundary of this condensation region is identical with the inlet plane of the secondary flow.

If Eqn. (6.20) is used to determine the extent of this region, then $h_{2,i-1}$ has to be replaced by the boundary enthalpy h_{2B} in the first case and by h_{2in} in the second case. The other boundary is determined by that point, where the primary wall temperature becomes equal to $T_{sat}(p_{Din})$.

In the following enthalpies and temperatures at the left boundary will be characterized by the index n and those at the right boundary (common to the region without condensation) by n+1. Thus

$$\begin{aligned} h_{2,i-1} &= h_{2,n} = h_{2B} \quad \text{in case 1, or} = h_{2in} \quad \text{in case 2} \; , \\ T_{G,i-1} &= T_{G,n} = T_{GB} \quad \text{in case 1, or} = T_{Gin} \quad \text{in case 2} \; , \end{aligned} \tag{6.24}$$

where T_{GB} is the primary temperature at the boundary.
From the energy balance Eqn. (3.36) follows

$$h_{2,n+1} = h_{2,n} - (mc_p)\,(T_{G,n+1} - T_{G,n})/m_2 \; . \tag{6.25}$$

The corresponding gas temperature at the boundary is given by

$$T_{G,n+1} = T_{sat}(p_{Din}) + q_{1,n+1}/\alpha_{1,n+1} \tag{6.26}$$

if $q_{1,n+1}$ is the local heat flux density and $\alpha_{1,n+1}$ the primary heat transfer coefficient at the boundary. Since at this point no latent heat is released, the single phase heat transfer coefficient valid for the adjacent region without condensation has to be taken.

To eliminate the heat flux density $q_{1,n+1}$, the equation for the energy transfer to the secondary side

$$q_{1,n+1} = \alpha_{eff,n+1} (T_{G,n+1} - T_{2,n+1}) \tag{6.27}$$

may be used, where $\alpha_{eff,n+1}$ is the local effective heat transfer coefficient according to Eqn. (3.32). The gas temperature at the boundary may then be written:

$$T_{G,n+1} = (\alpha_{1,n+1} T_{sat}(p_{sin}) + \alpha_{eff,n+1} T_{2,n+1})/(\alpha_{1,n+1} - \alpha_{eff,n+1}). \tag{6.28}$$

By inserting (6.28) into Eqn. (6.25), the following expression for the secondary enthalpy difference corresponding to the extent of the region is obtained:

$$h_{2,n+1} - h_{2,n} = \frac{(\overline{mc_p})_1 (\alpha_{1,n+1} (T_{sat}(p_{sin}) - T_{G,n}) - \alpha_{eff,n+1} (T_{G,n} - T_{2,n})}{(\overline{mc_p})_1 \alpha_{eff,n+1}/c_{pW} + (\alpha_{eff,n+1} - \alpha_{1,n+1}) \cdot m_2} \tag{6.29}$$

The extent of the heat exchanging area which is occupied by this condensation region is obtained, if this expression is inserted into Eqn. (6.20).

6.5 Solution procedure

The solution of the steam generator equations for prescribed inlet conditions requires an iteration procedure with the simplified model too if countercurrent flow is involved. The procedure is described in detail in Ref. /4/. The computational effort required by the simplified model is much less than that of the elaborate model as described in section 4. The main reason is that no nested iterations are required.

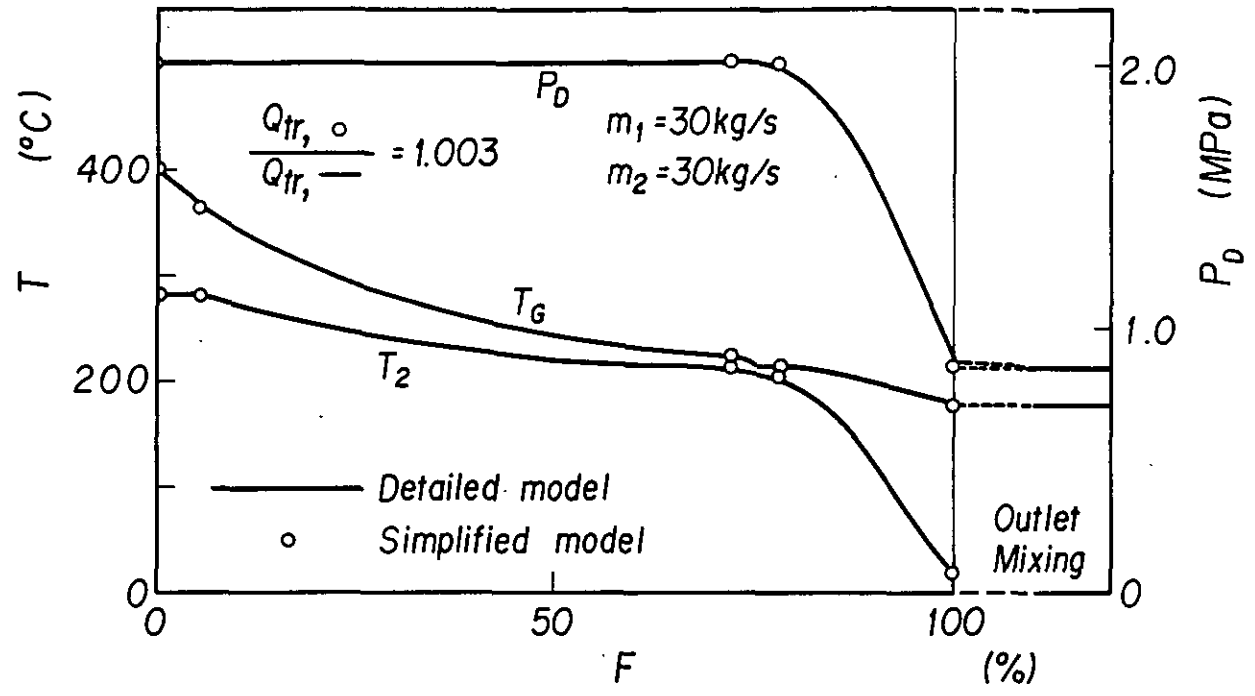

Fig. 12: Comparison of results from the simplified and the detailed model. Example 1

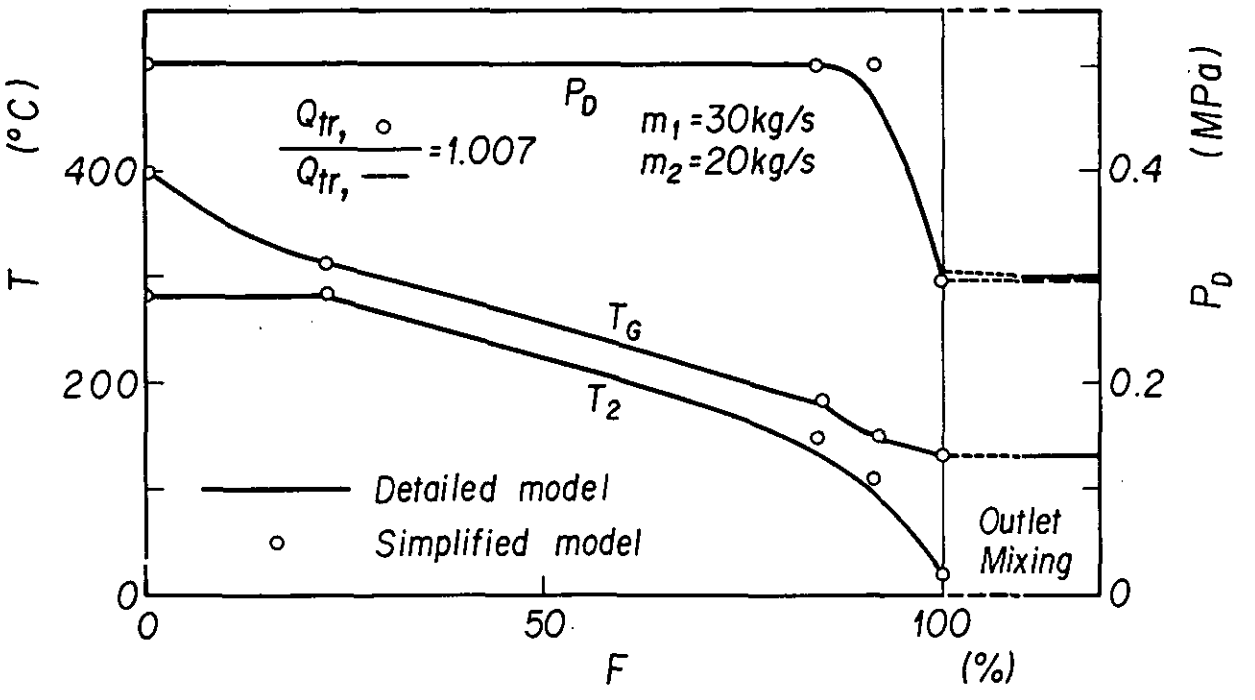

Fig. 13: Comparison of results from the simplified and the detailed model. Example 2

6.6 Comparative calculations

Figs. 12, 13 and 14 show the results of comparative calculations with the detailed and the simplified model. These figures show temperature and steam partial pressure distributions for the same set of data. Temperatures and steam partial pressures evaluated by the simplified model at region boundaries are shown as small circles.

The data underlaying these calculations are the same as those quoted in section 5 as far as they are not explicitly declared in the figures.

The agreement in the range without condensation on the primary side is exact since the multinode model and the variable boundary approach are based on equivalent algorithms. The deviations in the condensation region which result from the simplification are fairly small. Temperature deviations do not exeed a few degrees centigrade. The deviation of the transferred power is below one percent.

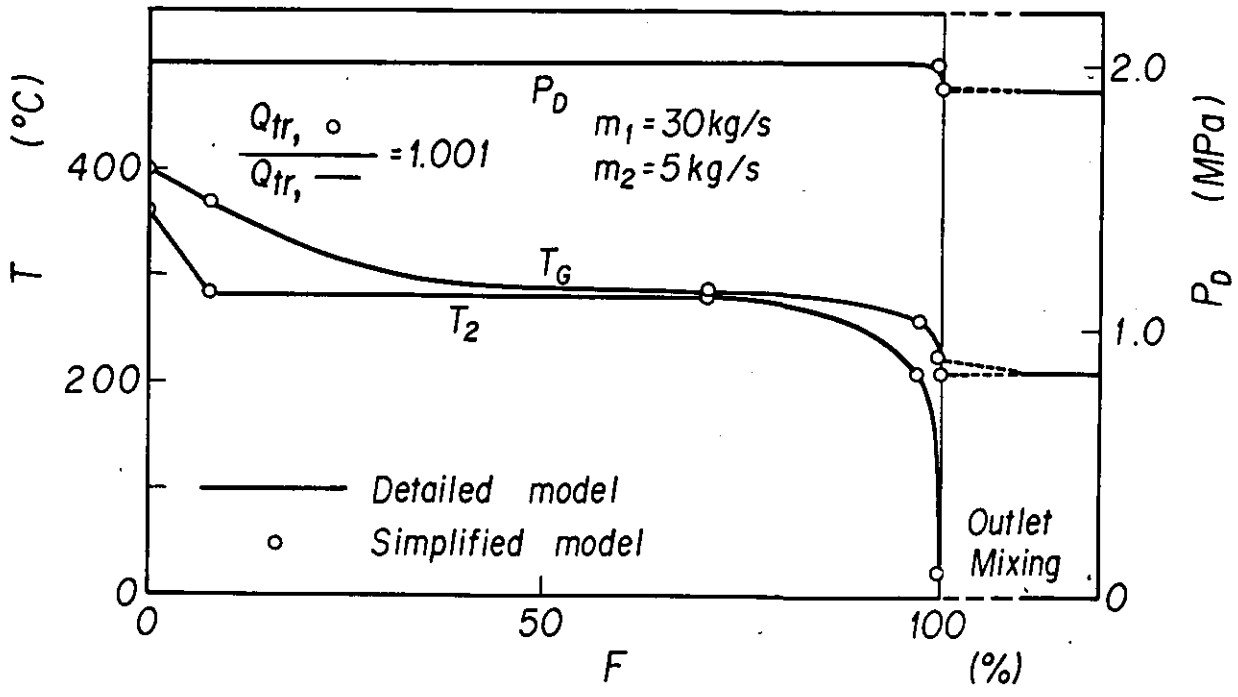

Fig. 14: Comparison of results from the simplified and the detailed model. Example 3

7. Concluding Remarks

1. A new calculation code was developed to analyse heat transfer in a steam generator for a high temperature reactor (HTR). The effect of steam condensation in the primary gas was taken into account. This was to analyse severe steam ingress accidents, where the condensation of the steam was expected to decrease the rate of pressure increase in the primary circuit.
2. Both the wall and the bulk condensation are taken into account. A hydrodynamic study was made for the condensate film and water droplets. It was found that the water film and the droplets will flow upward accompanied by the upward primary gas flow.
3. Entrainment of the condensate film was also considered. A new method was proposed to calculate the entrainment effect.
4. A special iterative procedure was developed to solve the heat transfer of the counter current system with condensation.
5. A parametric study was made to examine the effect of empirical parameters. The effect was found to be small in the range of parameters tested.
6. Main thermal resistance was found to exist in the primary gas. That of the water film was of much less importance.
7. Results of calculation with and without the condensation were compared. Difference was not so large for both cases as might be expected. The reason was discussed.
8. A simplified model was also developed. The simplified model may give results in good agreement with those by the detailed model in much less computation time. So, the simplified model is suittable to be built in a large accident analysis code system.

NOMENCLATURE

a	transverse pitch of tube bundle (see Fig.4a)
b	lateral pitch of tube bundle (see Fig.4a)
c_p	specific heat at constant pressure (kJ/kg K)
D	Diffusion coefficient (m^2/s)
d	diameter of tube (m)
d_w	effective thickness of tube (m)
F	force (N)
f_ψ	factor relevant to bundle geometry
g	gravity acceleration (m/s^2)
h	enthalpy (kJ/kg)
L	latent heat of phase change (kJ/kg)
M	molecular weight (kg/kmol)
m	mass flow rate (kg/s)
$\dot{m}$	mass flow rate density (kg/m^2s)
Nu	Nusselt number
P	Pressure (Pa)
p	pitch of tube bundle (m)
Q	film flow rate (m^2/s)
Q_{tr}	heat flow rate (kW)
q	heat flux (kW/m^2)
R	universal gas constant (kJ/kmol K)
Re	Reynolds number
Sc	Schmidt number
T	temperature (k)
u	velocity (m/s)
y	distance from wall (m)
z	parameter defined by Eq.(3.34)
α	heat transfer coefficient (kW/m^2K)
β	mass transfer coefficient (kg/m^2s Pa)
δ_F	film thickness (m)
ε	entrainment ratio
ν	kinematic viscosity (m^2/s)
λ	thermal conductivity (kW/mK)
ϕ	angle

ρ	density (kg/m^3)
ξ	friction factor
μ	viscosity ($N \cdot s/m^2$)
τ	shear stress (N/m^2)

Subscripts

B	bulk condensation
D	steam drag force
d	droplet
E	entrainment
eff	effective value
F	film
G	gas or gas and water droplets mixture flow
in	inlet
lat	latent heat
m	mean value
n	nth tube
NC	non-condensable gas
sat	saturation condition
sens	sensitive heat
turb	turbulence
W	water droplets
w	wall
wc	wall condensation
1	primary circuit
2	secondary circuit

Appendix I Mass Transfer coefficient

The mass transfer coefficient of steam in the steam-helium mixture is calculated following Ref.(1). The diffusion coefficient is given from the similarity between the heat and mass transfer as

$$\beta_D = \frac{\alpha \ \tilde{M}_D}{P^* \ c_{pm} \ \tilde{M}_m} \left(\frac{Pr}{Sc} \right)^{2/3}, \qquad \text{(Ia)}$$

$$P^* = (P_{N,w} - P_N)/\ell n(P_{N,w}/P_N)$$

α : heat transfer coefficient
Pr : Prandtl number
Sc : Schmidt number
c_{pm} : Heat capacity c_p of the mixture (kJ/kg K)
$\tilde{M}_m$: Molar weight of the mixture (kg/kmol)
$\tilde{M}_D$: Molar weight of the steam (kg/kmol)

The Schmidt number Sc is given as $Sc = \nu/D_D$. Where ν is the kinematic viscosity of the mixture and D_D is the diffusition coefficient of steam in the mixture gas. The diffiusion coefficient is further obtained as[1]

$$D_D = \frac{1.013 \cdot 10^{-7} \ T^{1.75} (\tilde{M}_D^{-1} + \tilde{M}_{He}^{-1})^{0.5}}{P_G \ (\nu_D^{*0.333} + \nu_{He}^{*0.333})^2} \quad (m^2/s) \qquad \text{(Ib)}$$

T : Temperature °K
$\tilde{M}$: Molar weight kg/kmol
ν^* : Nondimensional atomic volume; given in Ref.(3) as $\nu_D^* = 12.7$ and $\nu_{He}^* = 2.88$.

Other physical properties for the gas mixture are calculated also following Ref.(1).

Appendix II Heat Transfer Coefficient and Shear Stress

The Nusselt number for a rod bundle placed vertically to the flow is given in Ref.(1) as

$$\alpha = \frac{\lambda}{\ell} \, Nu_{bundle} \quad \text{with} \tag{II.1}$$

$$Nu_{bundle} = f_{\psi} Nu_0 \tag{II.2}$$

and $\ell = (\pi/2)\, d,$ (II.3)

where Nu_0 is the Nu for a single tube and f_{ψ} is the factor given in Ref.(1) relevant to the bundle geometry.

For Nu_0, the following equations are given:

$$Nu_0 = 0.3 + (Nu_{lam}^{\,2} + Nu_{turb}^{\,2})^{\frac{1}{2}} \tag{II.4}$$

and

$$Nu_{lam} = 0.664 \, Re^{0.5} Pr^{0.333} \tag{II.5}$$

$$Nu_{turb} = \frac{0.037 \, R_e^{\,0.8} P_r}{1 + 2.443 \, Re^{-0.1}(Pr^{2/3} - 1)} \tag{II.6}$$

$$Re = \frac{\tilde{u}\ell}{\nu} / (1 - \frac{\pi}{4ab}) \tag{II.7}$$

where $\tilde{u}$ is the velocity of gas without rod bundle. As for a, b, and d, see Fig.4(a).

The shear stress τ_w is obtained from the pressure drop for one pitch of the tube bundle as

$$\tau_w = \Delta P (a/\pi) \tag{II.8}$$

The pressure drop ΔP is given in Ref.(1) as

$$\Delta P = \xi \frac{d}{(4a/\pi - 1)(\pi/2)d} \frac{\rho}{2} u_m^{\,2} \tag{II.9}$$

where u_m is the mean velocity in the tube bundle. A relation between $\tilde{u}$ and u_m is

$$u_m = \tilde{u}/(1 - \pi/4a) \tag{II.10}$$

A value of the friction factor ξ is given graphically in Ref.(1) for various sets of a and b. For a usual design value of the steam generator, ξ can be approximated as

$$\xi = \begin{cases} 0.6 & \text{if} \quad 100/Re \leq 0.6 \\ 100/Re & \text{if} \quad 100/Re > 0.6 \end{cases} \tag{II.11}$$

By substituting Eq.(II.9) into Eq.(II.8), one obtaines the shear stress τ_w as follows.

$$\tau_w = \xi \frac{\rho}{2} u_m^2/2\pi(1 - \pi/4a) \tag{II.12}$$

References

(1) VDI-Wärmeatlas, Verein Deutscher Ingenieure, 3rd edition, VDI-Verlag (1977), Düsseldorf.

(2) Bird, R.B., Steward, W.E. & Lightfoot, E.N. "Transport Phenomena", John Wiley & Sons, (1960), New York.

(3) Reid, R.C., Prausnitz, J.M. & Sherwood, T.K. "The Properties of Gases and Liquids", Third ed., McGraw-hill, (1977), New York.

(4) G. Meister, A program module simulating a gas-heated steam generator with steam condensation in the primary flow channel. Jül-Spez-150 (1982).

List of Figures